Chapter 9

Biasing Effects in Ferroic Materials

Vladimir Koval, Giuseppe Viola and Yongqiang Tan

Additional information is available at the end of the chapter

http://dx.doi.org/10.5772/60764

Abstract

In this chapter we present an overview of some important concepts related to the processes and microstructural mechanisms that produce the deformation of hysteresis loops and the loss of their symmetry characteristics in ferroelectric, ferroelastic and ferromagnetic systems. The most discussed themes include: aging and fatigue as primary mechanisms of biased hysteresis loops in ferroelectric/ferroelastic materials, imprint phenomenon as an important biasing process in ferroelectric thin films, the development of an exchange bias field and of specific spin states, such as spin canting and spin-glass-like phases, as the main causes of biased hysteresis loops in different types of magnetic heterostructures. The present discussion leads to the identification of the main differences and possible analogies in the underlying mechanisms of possible biasing effects occurring in the different ferroic systems, which can benefit the theoretical description, modelling, and engineering of multifunctional devices based on ferroic systems experiencing the internal bias phenomena.

Keywords: Aging, fatigue, imprint, internal field, exchange bias

1. Introduction

Ferroic materials such as ferroelectrics, ferroelastics and ferromagnetics exhibit two or more possible equivalent stable states with uniform orientation of the spontaneous polarization, spontaneous strain and spontaneous magnetization in absence of an external electric field, mechanical stress and magnetic field, respectively. These thermodynamic equilibria correspond to minima in the free energy as a function of the order parameter (P – polarization, S – strain and M – magnetization). Under the action of external fields, these equilibrium states can

be switched from one to another, giving rise to symmetrical polarization-electric field (P-E), strain-stress (S-σ) and magnetization-magnetic field (M-H) hysteresis loops. It is often the case where two or more order parameters are coupled within the same phase and a change in one parameter produces a variation in another, as it occurs in multiferroic systems. The free energy profile can be influenced by many factors, such as compositional and structural inhomogeneity, defects, internal fields, thermal and loading history. These can induce preferential states of the order parameters, leading to the appearance of deformed and asymmetric hysteresis loops. The understanding of these biasing effects and the study of their possible advantages/disadvantages for specific applications, with the relative elaboration of strategies to induce/avoid them, is of crucial importance to maximizing the performance of functional devices based on ferroic systems.

The present chapter aims to provide an overview of different biasing effects which can occur in different types of ferroic materials, with particular focus on the phenomenology and on the underlying microscopic mechanisms of the anomalies observed in hysteresis loops. The chapter is organized in three main parts. The first part describes the distortions of P-E and S-E hysteresis loops in ferroelectric/ferroelastic materials. The two main phenomena, which cause biased hysteresis loops, namely aging and fatigue, are comprehensively reviewed by describing the most important features in bulk systems and the inherent microscopic mechanisms. Attention is also given to imprint phenomena in thin films, with description of the most important models developed to explain the shifting of the polarization hysteresis loops. The second part is focused on biasing effects in ferroelectric/ferroelastic materials under mechanical stress, with detailed description of the influence of composition, poling state and temperature on the stress-strain curves of perovskite systems. Additionally, biased stress-strain loops in shape memory alloys are also briefly reviewed, highlighting the different mechanical behavior of the martensite and austenite phases. This section is concluded with a summary on Bauschinger effect observed in ferroelastic materials during cyclic mechanical loading. The third and last part describes the biasing processes occurring in ferromagnetic materials, with the main focus on the asymmetric M-H loops caused by the exchange bias effect, and by the coexistence of different magnetic phases in inhomogeneous magnetic systems.

2. Ferroelectric materials

2.1. Deformations of hysteresis loop shape of ferroelectrics: pinching and asymmetries

The study of the hysteresis loops, namely current-electric field (I-E), polarization-electric field (P-E) and strain-electric field (S-E), is one of the most important tools to investigate the behavior and to assess the properties of ferroelectric/ferroelastic materials.[1-3] These curves usually show certain symmetry properties with respect to one or both the two axes, but they are susceptible to substantial modifications of their shapes, frequently observed in certain structures and compositions, which have undergone a certain thermal and electrical history. The most relevant examples of shape modifications of hysteresis loops are represented by *pinched loops* (constricted P-E loops in the region $E \approx 0$, remanent polarization approaching to zero), *asymmetric loops* (shift of the P-E loops along the E- and P-axis, suppression of left or

right wing of the S-E "butterfly" loop) and *polarization gaps* (relaxation of the remanent polarization at E = 0), which have been found in different ferroelectric/ferroelastic systems in both polycrystalline ceramics and single crystal. It can be generally said that these features can be caused by the development of an *internal bias field* E_{int}, whose magnitude and distribution depend on the composition/microstructure and on the thermal/electrical history of the system. In most cases, the presence of an internal field in ferroelectric materials can arise during processing (in this case often referred to as *built-in field*) or generated by two thermodynamic processes generally classified as *aging* and *fatigue*. They both share similar features, but they are triggered under different conditions and they can be influenced by different factors, as it will be discussed in the following sections.

2.2. Aging

2.2.1. Definition and introduction

The term *aging* in ferroelectric/ferroelastic systems usually refers to the process that produces variations of dielectric, piezoelectric and ferroelectric properties over time and in absence of an external field. These variations are usually undesired and the understanding of the controlling mechanism is crucial to maximize the performance of materials in most electronic applications. Although the prevailing microscopic mechanisms of aging are still under debate, there is a general agreement that aging is due to the stabilization of charged species or defect complexes in certain locations and configurations. Referring to the most common perovskites (ABO_3 chemical formula), aging is absent or weak in materials with high purity and in compounds in which the A- and B-site ions are partially substituted by donor species (i.e. soft compositions). On the other hand, aging phenomena are much more pronounced when the ions are partly replaced by acceptor dopants with a lower valence (i.e. hard compositions).[4]

The effect of aging often results in the presence of pinched P-E hysteresis loops schematically shown in Fig. 1a, and/or in one of the two possible cases of asymmetric P-E loops schematically shown in Figs. 1b and 1c. The internal bias field E_{int} can be estimated in each case using the position of the current peaks (Fig. 1) as [4]:

$$E_{int} = \frac{E_c^+ + E_c^-}{2} \tag{1}$$

where E_c^+ and E_c^- are the fields corresponding to positive and negative current neighboring peaks in the current-electric field (I-E) curve.

2.2.2. Effect of thermal and electrical history on the hysteresis loops

The presence of pinched and asymmetric hysteresis loops depends on the specific thermal and electrical history of the system. Fig. 2 shows the aging characteristics of CuO-modified $BaTiO_3$ ceramics.[5] It can be seen that unpoled aged ceramics display pinched P-E and S-E loops, while poled ceramics display asymmetric P-E and S-E hysteresis curves.

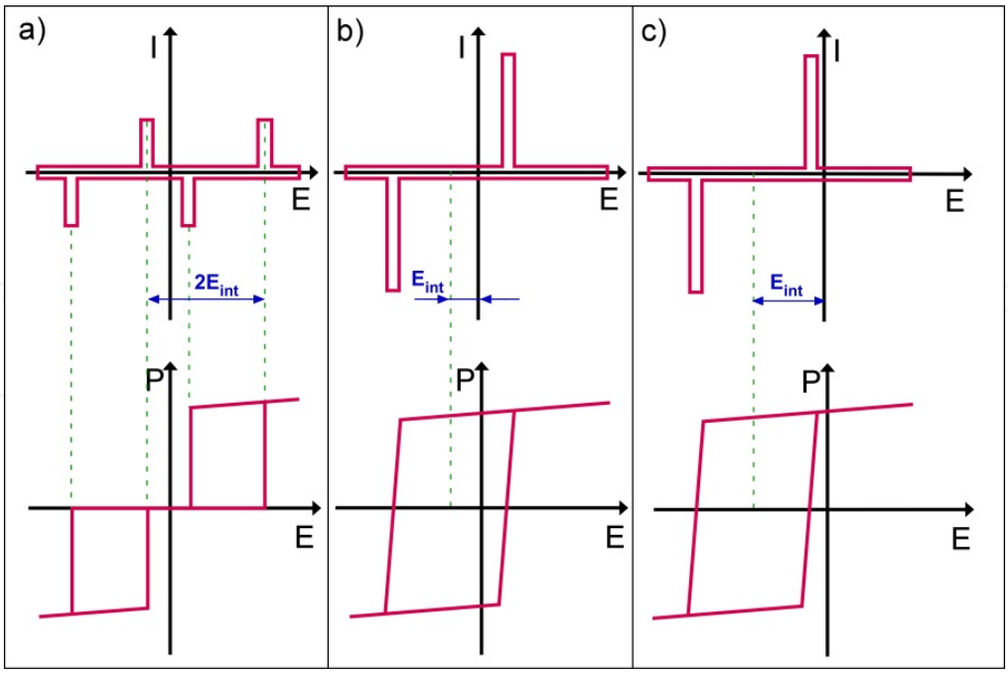

Figure 1. Definition of the internal bias field, E_{int}, in (a) pinched and (b, c) asymmetric P-E loops. After [4].

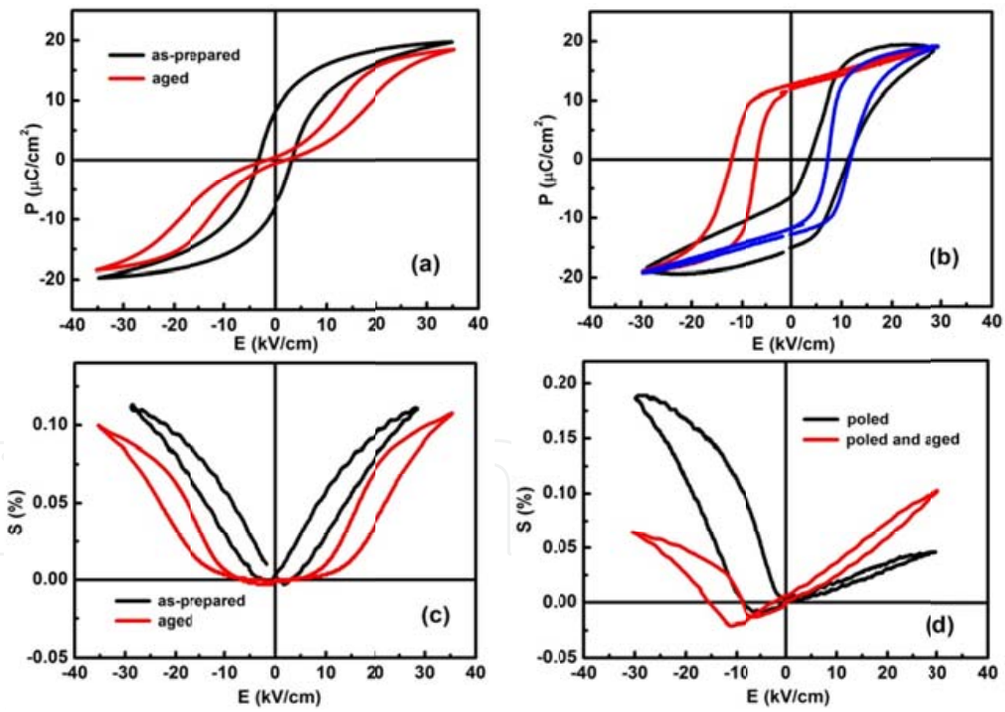

Figure 2. Hysteresis loops comparison of CuO-modified $BaTiO_3$ ceramics: (a) P-E loops of the as-prepared ceramics and aged ceramics (aging at room temperature for 24h); (b) the black line corresponds to a poled non-aged sample, red and blue curves are relative to poled and subsequently aged ceramics. The red curve was generated by applying a positive field parallel to the poling, while the blue curve was obtained with a positive electric field antiparallel to the previous poling field; (c) S-E loops of the as-prepared and aged ceramics; (d) S-E loops of poled non-aged, and poled and subsequently aged ceramics (positive field parallel to poling). After [5].

2.2.3. Microscopic mechanisms of aging

Three main microscopic mechanisms have been proposed for the origin of aging, namely a) *volume effect*, b) *domain effect*, and c) *grain boundary effect*. Up to the present, a definitive agreement on which mechanism is the main cause of the aging process has not been achieved, also due to the fact that often these mechanisms can possibly overlap.

a. Volume effect

According to the volume effect model, unintentional and intentional defects, which can be present in the system, are stabilized in preferred lattice sites, creating an internal bias that constrains the switching of the polarization along specific directions. One of the first micro-structural schemes of the volume effect model was proposed by Arlt and Neumann [6], and later extended by Ren with the *symmetry-conforming property of point defects*, which was used to describe aging phenomenon in different crystal structures [7]. According to the symmetry-conforming property principle, point defects (e.g., oxygen vacancies in acceptor-doped perovskites) distribute in the lattice with the same symmetry of the crystal structure, leading to a *defect dipole* P_D parallel to the spontaneous polarization (Fig. 3). During cooling from $T > T_c$ (T_c is a Curie temperature), the crystal structure abruptly changes into a lower symmetry structure stable at $T < T_c$, while the existing cubic structured defects are still arranged in their original symmetry. The reason is that the kinetics of defects migration is slower compared to the movement of ions driven by the phase transition. In the ABO_3 perovskite structure, the presence of an acceptor element in the B-site generates oxygen vacancies, which enable to accomplish charge neutrality. The lattice sites, where the defects can be located soon after cooling from $T > T_c$, are represented by the octahedron's corners, which all have the same probability of occupancy $\left(P_1^V = ... = P_6^V\right)$, as shown by the equal white proportions at the octahedron corners in Fig. 3a. However, over time, the defects tend to rearrange assuming the same symmetry of the crystal structure. The relaxation time of this process reduces with increasing temperature (in the range $T < T_c$), because thermal energy promotes short range migration of the defects towards a more stable configuration. After aging, the probability of occupancy for all the octahedron's corners is not the same anymore; the location with highest probability of oxygen-vacancy formation is the octahedron's corner that allows the formation of a defect dipole (acceptor ion-oxygen vacancy) parallel to the spontaneous polarization. In Figs. 3b, 3d and 3f, this location is identified by the octahedron corner with the largest white portion. Strong experimental evidence supporting the volume effect model against other aging mechanisms was obtained from targeted tests carried out on a single crystal-single domain of Mn-doped $BaTiO_3$.[8]

b. Domain effect

The domain effect model is based on the concept that mobile defects can diffuse towards domain walls to minimize the local depolarizing fields and may act as pinning agents on domain walls. By performing in situ high-energy X-ray Bragg scattering experiments during the application of an electric field, Tutuncu *et al.* [9] showed that in a pre-poled sample of $0.36BiScO_3$-$0.64PbTiO_3$, the volume fractions of domains oriented along the electric field is different when the electric field is increased along the previous poling direction and when

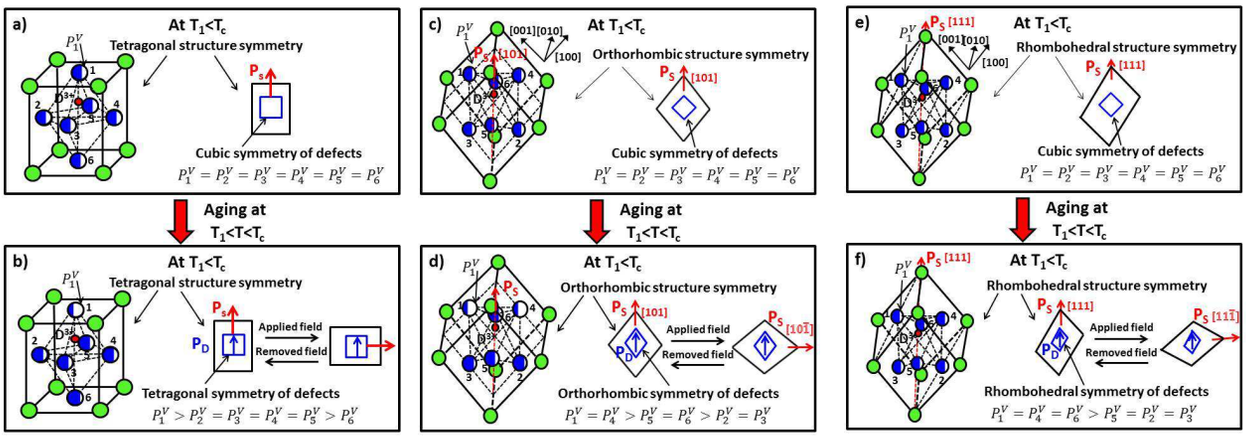

Figure 3. Scheme of symmetry conforming property of defects in different crystal structures: tetragonal (a, b); orthorhombic (c, d); rhombohedral (e, f). The scheme refers to the presence of an acceptor D^{3+} in the B^{4+} site of the ABO_3 perovskite-type compounds. After [7].

applied in the reverse direction. Indirect experimental proof of the domain effect model is based on the measurement of the dielectric permittivity and loss. Acceptor-doped aged systems usually show a reduction of permittivity and loss compared to the non-aged specimens. In early studies this was attributed to the clamping of domain walls due to the presence of an internal bias, which results in a reduction of the extrinsic contribution to dielectric loss.[10] Theoretical models based on the drift/diffusion of charge carriers, driven by the compensation of the depolarizing field and by the spatial gradient of their concentration, indicate that mobile charged species can migrate to domain walls and hinder domain wall movement.[11]

c. Grain boundary effect

The interface regions between dissimilar phases, such as undesired secondary phases, pores and electrodes, are often the location of space charge accumulation, which could represent another source of internal bias field responsible for deformations and asymmetries in hysteresis loops. Systematic investigations of the effect of impurities on the efficiency of the poling process have been presented in early reports [12], where it was proposed that in presence of certain impurity species the poling efficiency decreases due to the effect of space charges.

2.2.4. Rejuvenation or de-aging

The aged state is an out-of-equilibrium state and therefore it can be destabilized by several processes. These include: i) electrical bipolar cycles at sufficient amplitude; ii) heating/quenching from $T > T_c$ to $T \ll T_c$; iii) light illumination in some cases. The recovery process from the aged state results in the re-establishment of unbiased hysteresis loops, and is usually called *rejuvenation* or *de-aging*. The study of the kinetics of de-aging, either electric field-induced or thermally-induced, can contribute to further understand the microscopic mechanisms of aging.

2.2.4.1. De-aging by electric field cycles

The reduction of the internal bias field during de-aging by electrical cycling depends on: i) time exposure to the field (so frequency and number of cycles), ii) temperature, and iii) electric field amplitude. Early experiments on the kinetics of de-aging in acceptor-doped lead zirconate titanate (PZT) suggested that the de-aging is a thermally activated process.[10] The kinetics of internal field relaxation follows an exponential function of the type:

$$E_{int}(t) = E_{int}^{0} exp\left(-\frac{t}{\tau}\right) \quad (2)$$

where E_{int}^{0} represents the internal bias field before the electrical cycling and τ is the time needed for the relaxation of the internal bias. These two parameters can be obtained from the slope and the intercept of the $ln(E_{int}) - t$ plot. Carl and Hardtl [10] found that the activation energies in undoped PZT lie between 0.25 and 0.5 eV, those in specimens doped with Mn or Fe range between 0.6 and 0.7 eV, while that found in the Al-doped specimens is about 0.8 eV. The authors also noticed that these activation energy values are similar to the activation energy of the electrical conductivity and came to the conclusion that the mechanisms of aging/de-aging should be somehow connected to the property of electrical charges transport. This idea has been further explored by Morozov and Damjanovic [13], who performed a systematic study of charge migration processes in hard, undoped and soft PZT ceramics. They found that in hard compositions, the activation energy of alternating current (AC) conductivity is similar to the activation energy of the de-pinching process found by Carl and Hardtl in the same compositions. [10] It was concluded that the aging/de-aging process in acceptor doped ferroelectrics should be based on charge transport by the local movements of defect dipoles through short range migration of oxygen vacancies. The activation energy of long-range charge migration under constant electric field (DC conductivity) was found to be significantly larger.[13]

2.2.4.2. De-aging by heating-quenching

The aging effects can be relaxed by heating the system at $T > T_c$ and by subsequently quenching it to a temperature much lower than T_c. The heating process produces a thermal disordering of defects at high temperature and the quench allows keeping the defects in a disordered configuration also at lower temperatures. The relaxation of the internal bias in aged samples upon heating-quenching has been observed in several experimental studies; see for instance Ref. 14 among others.

2.3. Fatigue

The term *fatigue* in ferroelectric/ferroelastic materials indicates the degradation of the switchable polarization after a certain number of electrical cycles. Additionally, fatigue can determine the appearance of asymmetric loops due to the effect of biasing mechanisms, which induce preferential polarization and strain states. Besides, asymmetric hysteresis loops often observed in DC poled systems have been also classified in the literature as fatigue-like effects.[15] The biasing processes under repeated AC electric field cycles or DC poling fields depend in turn

on several other factors, such as the composition and stoichiometry of the material, temperature, geometry of sample and electrodes, electrical loading characteristics, including the electric field amplitude and frequency. Hence a succinct classification of the entire phenomenology becomes challenging.

2.3.1. Hysteresis loops after different types of fatigue-like loading

Fig. 4 shows the typical hysteresis loops observed after different types of fatigue-like electrical loading. Fig. 4a is relative to the effects of fatigue under unipolar AC electrical loading after 10^9 cycles on the bipolar P-E and S-E curves of $Pb_{0.99}[Zr_{0.45}Ti_{0.47}(Ni_{0.33}Sb_{0.67})_{0.08}]O_3$ (PIC 151) ceramics.[15] Fig. 4b shows the P-E and S-E bipolar loops of $0.94Bi_{1/2}Na_{1/2}TiO_3$–$0.06BaTiO_3$ (0.94BNT-0.06BT) after 1, 10^4 and 10^7 electric field bipolar cycles.[16] Fig. 4c displays the bipolar P-E and S-E curves of PZT 4D ceramics previously poled under a DC poling field of ± 2.5kV/mm applied at T = 125 °C for 5 minutes.[17] It can be seen that the sign of the DC poling field significantly affects the shape of the P-E and S-E loops. In particular, samples pre-poled under positive DC field show P-E loops shifted towards left and S-E loops with a suppression of the left wing; opposite effects can be noticed in samples poled under negative DC field. However, it is worth recalling that to correctly establish the sign and value of polarization and strain in samples subjected to previously electrical loading, polarization and strain must be monitored for the entire electrical history. During DC poling of PZT 4D, polarization and strain were not monitored, therefore, the sign and values in Fig. 4c have relative validity; only the polarization and strain amplitudes are meaningful. Fig. 4d shows the P-E and S-E curves of $BaTiO_3$ ceramics sintered at different temperatures after one loading-unloading cycle up to approximately 3 kV/mm field amplitude and 10 Hz frequency. It can be concluded that the deformation of the hysteresis loops is caused by the presence of an internal bias field which forces the systems into preferred polarization and strain states.

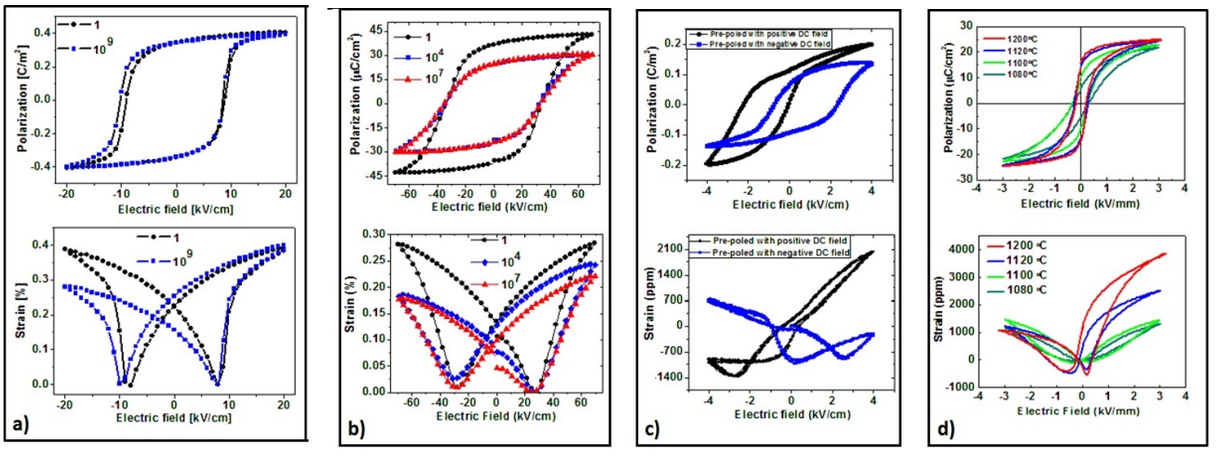

Figure 4. Fatigue-like effects on P-E and S-E hysteresis loops: (a) after unipolar electrical fatigue cycles in PIC 151 ceramics, courtesy of N. Balke, after [15]; (b) after unipolar electrical fatigue cycles in 0.94BNT-0.06BT ceramics, courtesy of Z. Luo, after [16]; (c) PZT 4D after DC poling of 2.5kV/mm applied for 5 minutes at 125°C [17]; (d) after one AC poling cycle in $BaTiO_3$ ceramics sintered at different temperatures [17].

2.3.2. Formation of cracks

Fatigued specimens often show the presence of microcracks, although it is hard to establish whether microcracking is a cause or a consequence of fatigue. It has been conveyed that microcracking can occur in samples with low density, in compositions with large grain size, with large unit cell distortion, and in compositions near the phase boundaries, where electric field-induced transitions can be activated during electrical loading [18]. In addition, macroscopic cracks can develop in the interface region between sample and electrode. In particular, two types of cracks were observed in $Pb_{0.99}[Zr_{0.45}Ti_{0.47}(Ni_{0.33}Sb_{0.67})_{0.08}]O_3$ ceramics: i) *edge cracks* (propagating obliquely from the electrode inside the material) and ii) *delamination cracks* (forming beneath the electrode and propagating parallel to the electrode during bipolar cycling. The latter appear at a later fatigue stage than the former due to a reduced amount of switchable domains during fatigue.[19]

2.3.3. Fatigue effects in soft and hard compositions

A number of studies have been devoted to the understanding of fatigue effects in soft and hard ferroelectric compositions, but at present the differences in bulk materials are not completely understood mainly due to the fragmentary character of the published literature often presenting contradicting results. For PZT bulk ceramics [20], it was found that soft composition samples (sintered from commercial PZT 5A powder obtained from Morgan Electroceramics Inc.) exhibited a faster fatigue degradation compared to that of the hard PZT ceramics (sintered from commercial APC-841 powder obtained from American Piezoceramics Inc.). For $BaTiO_3$ bulk ceramics, it was shown that a partial substitution of Ti^{4+} ions in the B-site with donor species (e.g., Nb^{5+} ions) leads to a higher fatigue strength compared to that of the acceptor-doped (Ca^{2+} and Al^{3+}) and of the undoped specimens.[21] This is in agreement with the concept that fatigue characteristics can be improved by reducing the content of oxygen vacancies. On the contrary, the addition of Fe-acceptor in the B-site of $[(Na_{0.5}K_{0.5})_{0.96}Li_{0.04}][(Nb_{0.86}Ta_{0.1}Sb_{0.04})_{1-x}Fe_x]O_3$ ceramics has produced improved fatigue characteristics.[22] This effect was attributed to the increased mechanical strength of the grain boundaries upon Fe addition, which had overcome the effect of the expected increase of the oxygen vacancies content due to the presence of the electron acceptor species.

2.3.4. Fatigue effects in relaxors

Fatigue effects in relaxor materials can be different from those of ferroelectrics in terms of phenomenology and microscopic origin.[23] Additionally, non-ergodic and ergodic relaxors have shown different electrical fatigue characteristics. In non-ergodic relaxors, a long-range ferroelectric order is stabilized after the application of a sufficiently large electric field and polarization reversal occurs during further electric field cycles. Ergodic relaxors undergo a weakly polar-to-polar state transition during electrical loading and they return into the weakly polar state during electric field unloading. This behavior has been widely observed in several bismuth-based perovskites.[24-27] The $0.94(Bi_{0.5}Na_{0.5})TiO_3$-$0.06BaTiO_3$ (BNT-BT) system can be classified as a non-ergodic relaxor. An addition of $K_{0.5}Na_{0.5}TiO_3$ to BNT-BT determines a crossover to an ergodic relaxor behaviour, which can be observed also at room temperature.

The non-ergodic relaxor BNT-BT has shown domain fragmentation during fatigue [28], while the ergodic compositions exhibit significantly higher fatigue resistance [27]. The current understanding is that the domain wall pinning effects become less significant in ergodic relaxor phases.[23] In addition, it can be considered that the ergodic relaxors return to a weakly polar state with low remanent polarization and low remanent strain during electric field unloading. This yields smoother variations of polarization and strain during cycling, which could probably be one of the reasons of the less pronounced fatigue effects. However, further studies are needed to better elucidate the mechanisms of the increased fatigue resistance in lead-free ergodic relaxors.

2.3.5. Microscopic mechanisms of fatigue-like effects

Macroscopic fatigue-like effects such as asymmetric hysteresis loops are often similar in different material systems, possibly due to a common origin represented by the presence of an internal bias field. However, the microscopic origin of the internal bias could be different in different systems and strongly dependent on the type of electrical loading.

2.3.5.1. Development of an internal bias

It is well known that domain switching occurs through a nucleation-growth process of reversed domains driven by the *local electric field* $E_{loc}(r, t)$, which is given by the sum of the following fields: i) the external applied electric field E_{app}; ii) the *depolarization field* $E_{dep}(r, t)$ due to the polarization changes produced by the formation of reversed nuclei (nucleation) at the location r and time t during the application of the external field E_{app}; iii) the sum of the *screening fields*, which can be divided into: a) *external screening field* $E_{es}(r, t)$ produced by free charges on electrodes, and b) *bulk screening field* $E_{bs}(r, t)$ caused by the rearrangement of charge carriers in a ferroelectric [29]:

$$E_{loc}(r,t) = E_{app} - \left\{ E_{dep}(r,t) - \left[E_{es}(r,t) + E_{bs}(r,t) \right] \right\} \tag{3}$$

In an ideal case of a perfectly insulating poled ferroelectric placed between two conductive plates of a capacitor, the polarization bound charges in the ferroelectric will cause an accumulation of free electronic charges on the electrodes in the region nearby the ferroelectric to counterbalance the polarization charges, thereby leading to the presence of *a depolarizing field* inside the ferroelectric. By short circuiting the capacitor plates, the compensation charges will flow within the circuit in such a way that the depolarizing field disappears (*the external screening*). In real ferroelectric capacitors, however, the electrodes are not perfect conductors and the ferroelectric would present the so called *dielectric gaps* in the interior and close to the interface with the electrodes, where the spontaneous polarization is significantly suppressed or absent. [30] The presence of dielectric gaps determines a separation between the compensation charges and the polarization bound charges in the ferroelectric. The former become trapped at the dielectric gap-ferroelectric interface forming a space charge layer, which, together with the polarization bound charges in the ferroelectric, generates a *depolarizing*

field, which can only be partially compensated by external screening in the short circuit condition. The time constant of the external screening process is determined by the parameters of the external circuit and it is typically in the order of micro/nano seconds. [30] The unscreened part of the depolarizing field in the interior of the ferroelectric, *a residual depolarizing field* E_{res}, is antiparallel to the polarization, and triggers the so called *bulk screening process*, which involves a rearrangement of the charge carriers inside the ferroelectric to reduce the residual depolarizing field. The bulk screening process can occur through: i) redistribution of charge carriers, ii) alignment of dipolar defects, or iii) irradiation-induced charge injection. The time constant of the bulk screening process is typically several orders of magnitude higher than that of the external screening and it often exceeds the switching time of the ferroelectric polarization. Therefore, the separated and trapped screening charges at the gap/ferroelectric interface can cause an internal bias field which points in the direction of the polarization.

In uniaxial ferroelectric ceramics where the dipolar defects are constrained, the main physical mechanism responsible for aging and fatigue phenomena is attributed to the compensation of the residual depolarizing field through the redistribution of the screening charges. The idea employed in this scenario assumes that free charges present in the material migrate to minimize the depolarizing field with the consequent development of an internal bias field that hampers domain wall movement and generates biased polarization and strain states (Fig. 5). Balke *et al.* [30] proposed that the depolarizing field E_{dep} surrounding a given grain in samples fatigued under an applied field E_{app} can be estimated as:

$$E_{dep} = -\alpha_{angle} \frac{\Delta P}{\varepsilon_0 \varepsilon_{33}} \tag{4}$$

where ΔP is the variation of polarization during the increase of the applied field from $E = 0$ to $E = E_{app}$ and ε_{33} is the permittivity at $E = E_{app}$. The factor α_{angle}, which can assume only values between 0.15 and 0.5, takes into account the partial compensation of the depolarization field based on the orientation of the polarization in neighboring grains. This model was able to predict the range of internal bias fields observed in DC poled samples of $Pb_{0.99}[Zr_{0.45}Ti_{0.47}(Ni_{0.33}Sb_{0.67})_{0.08}]O_3$ at room temperature.[11, 30] Additionally, this mechanism was invoked to explain the fatigue-like effects after unipolar cycling in $Pb_{0.99}[Zr_{0.45}Ti_{0.47}(Ni_{0.33}Sb_{0.67})_{0.08}]O_3$ at room temperature [11] and it can be also applied to rationalize the biasing effects observed in DC poled hard piezoceramics, as shown in Fig. 4c.

In the case of bipolar fatigue, the bulk screening process under an alternating electric field leads to an inhomogeneous internal field distribution, which yields the development of the so called *frozen domains*. These get locked and do not switch after a certain number of electric field cycles, giving rise to heterogeneous fatigue effects. The value of $E_{bs}(r, t)$ in the Eq. 3 is determined by the sample history, including sintering/annealing, the subsequent deposition of electrodes, electrical cycles characteristics (frequency and time exposure) and time intervals between cycles.[31] These factors have been taken into account in the *kinetic imprint approach*, which was successfully employed in describing the hysteresis loops after fatigue in different materials. [32]

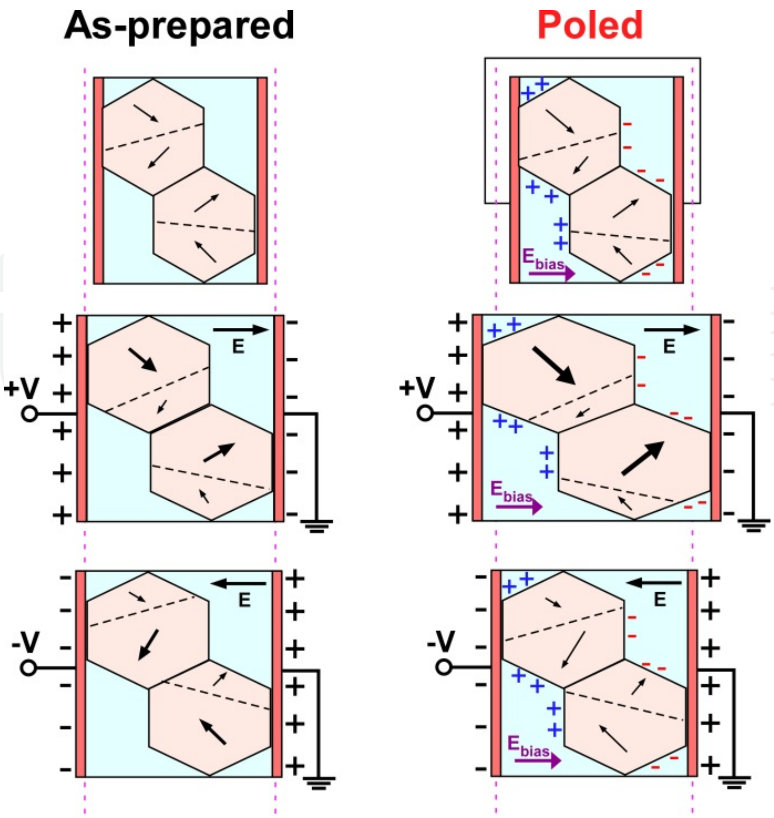

Figure 5. Schematic of the formation of an internal bias after poling.

2.4. Imprint and biasing effects in ferroelectric thin films

An internal field developed by charged defects is believed to play an important role in the *imprint phenomenon* in ferroelectric thin films. Imprint generally refers to the preference of a certain polarization state, the so called "hard" state, over the other "ease" state in ferroelectric bi-stable states. The preferential polarization may be induced within the ferroelectric by locking-in a particular domain orientation during electrical, thermal or optical (UV light) treatments.[33] The latter two effects are customarily called *thermal imprint* and *optical imprint*.

The polarization imprint of ferroelectric thin film capacitors, which manifests itself macroscopically by a shift of the polarization hysteresis loop along the electric field axis (Fig. 6), is one of the most serious reliability issues for ferroelectric nonvolatile memories applications. An incomplete polarity reversal of the ferroelectric thin film, which also gives rise to an asymmetry in the remanent polarization and an effective variation of the coercive field, can lead to either "read" or "write" failure of the memory cell.[34] The voltage offset of the imprinted loop is often used as a measure of imprint. The sign of the field offset determines the direction of the preferential polarization in the interior of the ferroelectric thin film capacitor.

An asymmetric hysteresis behavior has also been reported for as-grown ferroelectric thin films in an initial state, i.e. without heat treatment, ultraviolet radiation or application of an external electric field.[35] However, unlike the preferred polarization generated from capacitor

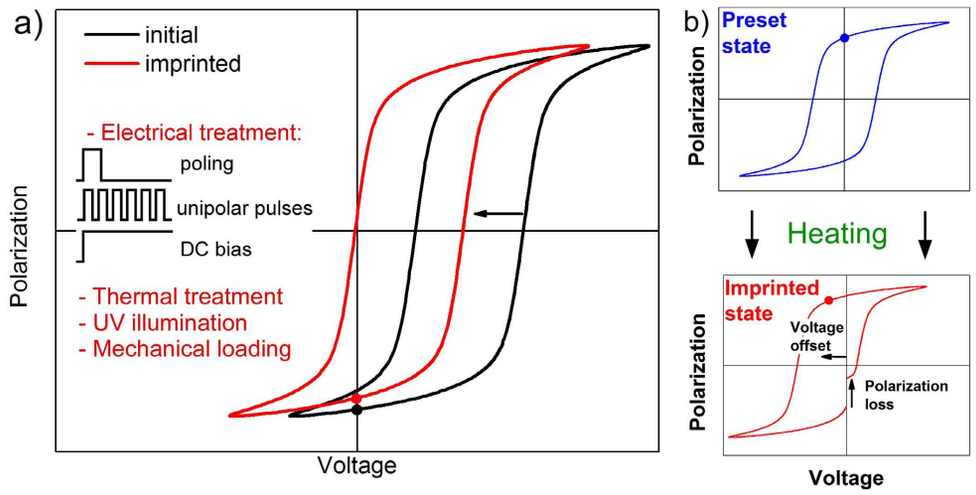

Figure 6. (a) Shift of polarization of a ferroelectric in the negative state of remanent polarization due to imprint. (b) Thermal imprint – polarization loss due to shift of the P-E hysteresis loop on heating.

structure, an internal bias field develops in these films intrinsically during the fabrication process. The built-in bias does not vary during switching, instead it provokes polarization back switching and causes the *retention loss*, i.e. a gradual decrease of the remanent polarization with time in poled ferroelectric capacitors. Optical and thermal imprint have been shown to improve the retention performance or aging in PZT film capacitors.[36]

2.4.1. Physical models of imprint and microscopic mechanisms for asymmetrical switching

In the last two decades, several phenomenological scenarios and microscopic models have been proposed in the literature to explain the asymmetric switching behavior and the related imprint phenomena in ferroelectric thin film capacitors. Among them, two mechanisms seem to be able to consistently describe the polarization imprint and its dynamics: the *defect-dipole alignment model* [37] and the *interface screening model* [38].

a. Defect-dipole alignment model

There have been several indications that defects play an essential role in polarization degradation phenomena in bulk ceramics. To explain the interplay between the voltage shift, defects and polarization, Warren *et al.* [39] proposed the concept of aligning defect dipoles and their involvement in the aging process. By using electron paramagnetic resonance they demonstrated that the defect dipoles in $BaTiO_3$ ceramics align along the direction of the spontaneous polarization. The asymmetric distribution of trapped charge and the alignment of defect dipoles near the electrode-ferroelectric interface have been suggested to be responsible for the imprint phenomena in ferroelectric thin film capacitors.[37] The dominating role of defect dipole alignment for producing internal bias field in PZT films was evidenced by the reduction of the thermally induced voltage shifts upon donor doping at the (Zr, Ti) sites. Similar findings on donor (La^{3+}) doping effects have been also reported by Kim *et al.* [40], and the improved imprint behavior of La-doped PZT films was attributed to the reduction of the concentration

of defect dipoles induced by the doping. Recently, Folkman *et al.* [41] by monitoring the built-in bias field in epitaxial $BiFeO_3$ thin films have shown that the defect dipole pairs can realign and ultimately disassociate upon electrical cycling. The gradual dissociation of complex oxygen vacancy defects was accounted for a drastic reduction in the built-in bias field and an improvement of imprint characteristics of the films as measured after 10^4 cycles.

b. Bulk and interface screening models

In contrast to Warren's and Kim's observations [37, 40], the results obtained by Grossmann *et al.* [38] showed only a slight or negligible impact of Nb and Fe addition on the hysteresis and imprint behavior of PZT capacitors. Instead, the experiments with ultraviolet illumination revealed an enhancement of the polarization imprint of the PZT films. It was proposed that the redistribution of electronic species, such as electrons and/or holes, might be the main cause for the imprint phenomena in ferroelectric thin film capacitors, and the defect dipole alignment, if any, is only a secondary imprint mechanism.

Currently, there are two reasonable approaches explaining the imprinted hysteresis loops of ferroelectric capacitors within the general concept of generation, separation and subsequent trapping of electronic charges: the *bulk screening model* [42] and the *interface screening model* [38]. Both models assume the existence of a thin layer at the interface between the electrode and ferroelectric in which the spontaneous polarization is absent or suppressed. However, they differ in modeling the driving force responsible for the charge separation. In the bulk screening model, the driving force is thought to be the *residual depolarizing field* (E_{res}) generated in the interior of the film due to incomplete cancellation of the space and polarization charges by free electronic (screening) charges on the electrodes.

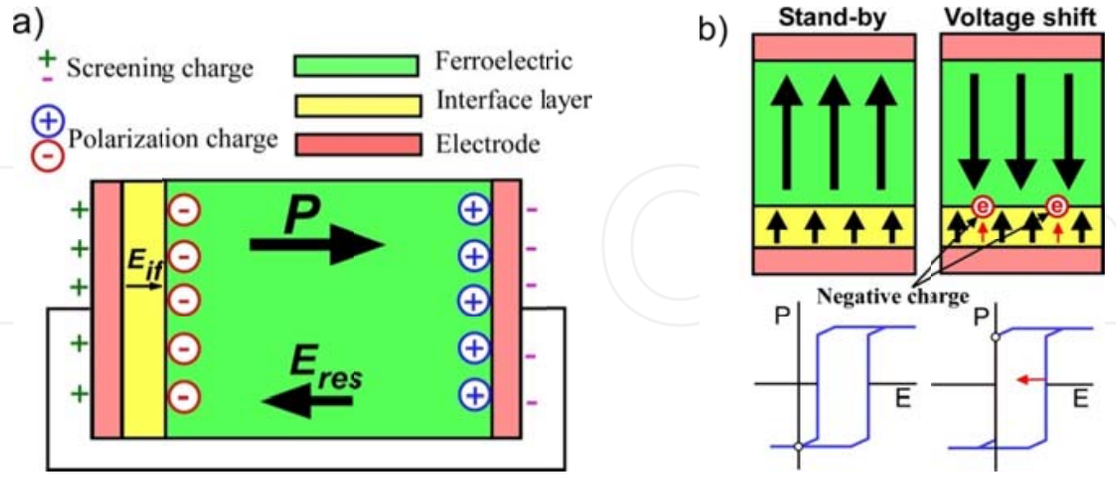

Figure 7. (a) A sketch of ferroelectric thin film capacitor under imprint experiment, and (b) a voltage shift of the imprinted thin film capacitor according to the interface screening model. Reproduced with permission from Abe *et al.* [48]. Copyright 2002, AIP Publishing LLC.

The concept employed in the interface screening model suggests that the imprint effects might have originated from a large electric field E_{if} that develops within the interface layer of the

ferroelectric thin film capacitor during the accelerated aging (Fig. 7). This field points in the direction of the polarization and in the opposite direction of the E_{res} field. A gradual shifting of the polarization hysteresis loop is thought to be governed by E_{if} due to the consecutive trapping of electronic charges injected from the electrode into the film. As shown in Figure 7, the injected charges have a polarity that is opposite to the dipole of the ferroelectric, hence, the induced internal field screens the external electric field and a higher applied voltage is required to induce polarization reversal. The experimental observations presented in Ref. 38 indicate that imprint in ferroelectric thin films is governed by the magnitude and orientation of the ferroelectric polarization and the voltage shift follows the direction of the polarization.

Within the interfacial screening model, several charge injection mechanisms have been suggested for the imprint phenomena in ferroelectric capacitors, including the *field enhanced thermionic emission* from the electrodes *(Schottky effect)* and *Pool-Frenkel emission* from traps. The Schottky emission current density can be expressed as follows [43]:

$$J_S = A^* T^2 \exp\left(\frac{-q\varnothing_B}{k_B T}\right) exp\left(\frac{q\Delta\varnothing_S}{k_B T}\right) \tag{5}$$

where A^* is the effective Richardson constant, q is the eletronic charge, k_B is the Boltzmann constant, T is the absolute temperature, and $q\phi_B$ is the Schottky barrier height (i.e., conduction band offset). $\Delta\varnothing_S$ denotes the barrier lowering:

$$\Delta\varnothing_S = \sqrt{\frac{qE}{4\pi\epsilon_r\varepsilon_0}} \tag{6}$$

where E is the applied electric field, ε_0 is the vacuum permittivity and ε_r is the dynamic dielectric constant of the ferroelectric.

The equation implies that the interfacial-layer charge injection due to thermal emission is exponentially proportional to the barrier lowering, which is dependent on the applied electric field. The standard quantitative expression for the Poole-Frenkel effect is [44]:

$$J \propto E\, exp\left(\frac{-q\left(\varnothing_B - \sqrt{qE/\pi\epsilon_r\epsilon_0}\right)}{k_B T}\right) \tag{7}$$

According to Eq. 7, the displacement of the polarization hysteresis loop along the field axis is expected to be independent of the film thickness, and the voltage offset would increase as the thickness of the sample increases. This effect has been experimentally evidenced in ferroelectric thin film capacitors with variable thickness.[45, 46]

Although the bulk screening model reasonably explains the imprinted hysteresis loops for films illuminated by UV light during poling, it cannot describe an enhancement of the

polarization imprint under external bias, as observed by Grossmann *et al.* [38]. The scenario proposed in the interface screening model has consistently and repeatedly been successful in describing, both qualitatively and quantitatively, a wide variety of experimental data on imprint behavior of ferroelectric thin film capacitors, including a logarithmic-type time dependence of imprint [47] and the effects of temperature, illumination and of an externally applied bias [36, 38, 42].

2.4.1.1. The surface layer(s)

The idea of the existence of a surface layer with suppressed ferroelectric properties implemented in physical models has demonstrated considerable advantage in explaining asymmetric switching and other anomalies in the behavior of ferroelectric materials. In the models, the interface thin layer is considered as *a non-switchable "dead" layer* [48], *a space charge layer* [49], *a low-dielectric constant layer* [50] or *an insulating region* [51] adjacent to the electrode. Pertsev *et al.* [46] have shown that in ultrathin PZT films the nearby-electrode layer does not behave as an insulator, and proposed that a finite electrical conduction exists in this layer. Also, Tagantsev *et al.* [52] have indicated that the anomalous hysteresis behavior displayed by ferroelectric thin film capacitors might be caused by the effect of a conductive non-ferroelectric layer, the so-called "*passive layer*", formed at the interface between the film and electrode. This layer is supposed to behave as a space charge layer (charged positively or negatively), operating as a serial capacitor connected to the film capacitor. A high electric field in the surface layer will cause charge transport across it, resulting in charge separation. The built-in potential developed by the trapped and separated charges in the layer due to depletion effects at the ferroelectric-electrode contacts would prevent polarization reversal to occur in a symmetrical manner, even though the driving voltage is perfectly symmetrical.[49]

A direct evidence of an oxygen-deficient surface layer in epitaxial (Ba, Sr)TiO_3 [50] thin films and Pb(Zr, Ti)O_3 nanostructures [53] has been provided using high-resolution transmission electron microscopy. However, the origin of these layers remains yet to be elucidated. Some researchers connected it with *a partial depletion* [54] or *exhaustion* of charge carriers at the Schottky contacts [52], while others related the existence of the surface layer to extrinsic effects such as *structural disordering* [49, 55], *chemical inhomogeneity* (e.g., oxygen deficiency) [41] or *mechanical distortion* [50]. Abe *et al.* [48] have proposed, based on measurement of switching currents in the heteroepitaxial $BaTiO_3$ thin films, that the passive layer is possibly formed by the relaxation of lattice misfit strain developed during film growth. The existence of the interfacial stresses due to elastic interface deformations in thin films has been evidenced by Spaepen [56]. The oxygen-loss related strain gradient at the interfaces of the PZT capacitor was also reported by Wu *et al.* [57]. The role of strain gradients in the asymmetric hysteresis behavior will be discussed in the following section.

2.4.2. Mechanical stress effects

It is well established that internal mechanical stresses and their effects on domain-wall movement are the main cause of the significant difference between the physical properties of ferroelectric thin films and bulk ceramics. Experimental results presented in the literature show

http://dx.doi.org/10.5772/60764

that the *residual stresses* developed in the films during fabrication are often larger than hundreds of megapascals and create a considerable clamping effect on domains, thereby hindering polarization switching.[58] The misfit strains arising from the mismatch of the lattice parameters and the coefficients of thermal expansion of the underlying substrate and thin film can lead to the lattice distortion or formation of *misfit dislocations* (Fig. 8), which in turn causes the creation of a lattice strain gradient across the film. This strain gradient may induce a linear polarization response through the *flexoelectric effect*.[59] Tuttle *et al.* [60] have reported that the sign of the film stress at the Curie point controls the orientation of the domain structure, and hence the flexoelectric effect, unlike piezoelectricity, can trigger switchable polarization. Under certain misfit strain-temperature conditions, a strong coupling between the polarization and the stress field of the dislocation can appear, resulting in spatial inhomogeneity of the polarization near the dislocation (Fig. 9).[61] These polarization gradients produce the accumulated interfacial charge, which allows for the development of the internal bias field.

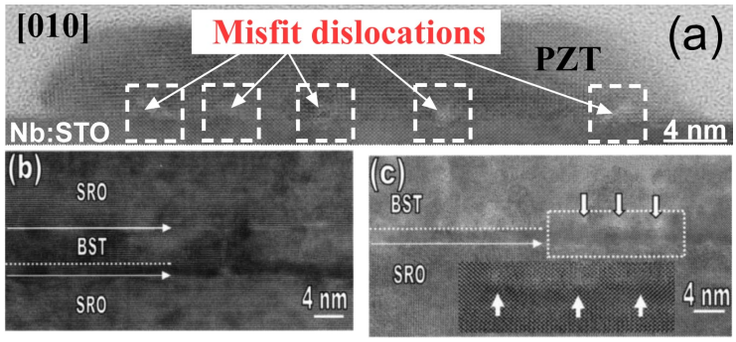

Figure 8. High-resolution TEM cross-sectional images of the interfacial layer in the PZT nanostructure (a) and $Ba_{0.7}Sr_{0.3}TiO_3$ thin films (b, c) showing a significant distortion of the ferroelectric lattice around the dislocation cores (labelled by arrow tags). Reproduced with permission from D. Hesse [53] and He *et al*. [50]. Copyright 2005, AIP Publishing LLC.

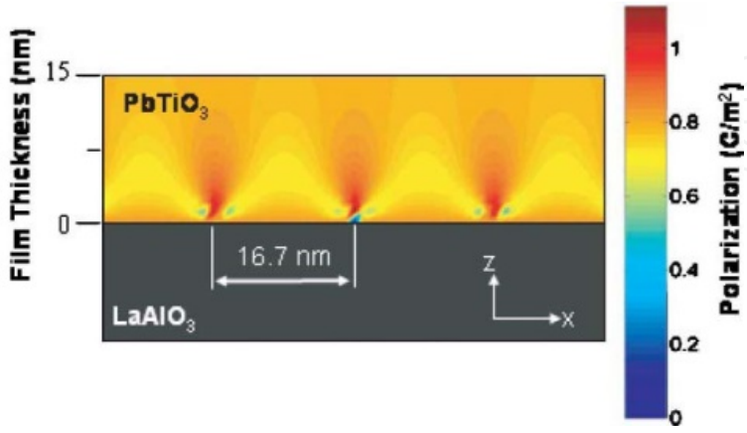

Figure 9. Spatial inhomogeneity of the ferroelectric polarization around periodic misfit dislocations due to a strain gradient in a $PbTiO_3$ film on a $LaAlO_3$ substrate. Reproduced with permission from Alpay *et al*. [61]. Copyright 2004, AIP Publishing LLC.

Stress-induced changes in the local asymmetric switching behavior and piezoelectric properties of the sol-gel $Pb(Zr_{0.30}Ti_{0.70})O_3$ and Mn-doped $Pb(Zr_{0.30}Ti_{0.70})O_3$ ferroelectric films have been investigated by Koval *et al.*[62] A modified nanoindentation system with a conductive spherical indenter tip was used for the simultaneous application of driving voltage and mechanical loading. It was shown that the switching charge versus applied voltage (Q-V) hysteresis loops shift gradually along the voltage axis with increasing indentation force (100 – 500 mN). The effect of spherical nanoindentation on the asymmetric switching behaviour is shown in Fig. 10a, which compares the Q-V loops obtained at different indentation loads for the Mn-doped PZT (PMZT) film. In addition, a progressive hysteresis gap of the charge – voltage loops is displayed in the figure inset. The parameter of horizontal loop asymmetry δ (Fig. 10b) was found to increase almost linearly with the force by an increment of about 0.4-0.5 $x10^{-3}$ per 100 mN during the application of a sinusoidal signal of 25 V-, 37 V- and 50 V-peak drive voltages and 50 Hz frequency.

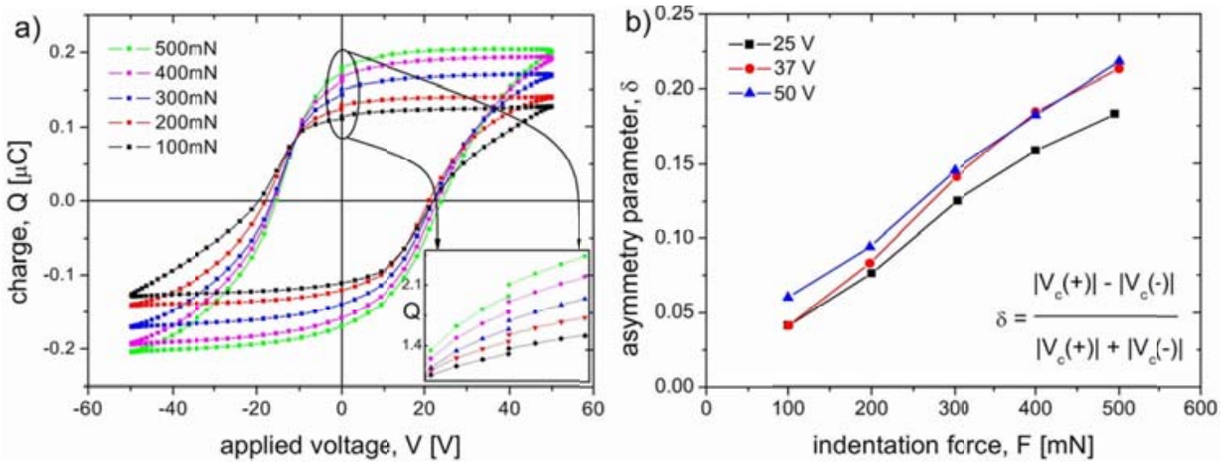

Figure 10. (a) The voltage shift and (b) the asymmetry parameter of the Q-V hysteresis loop of the Mn-doped PZT thin film under nanoindentation. Reproduced with permission from Koval *et al*. [62]. Copyright 2005, AIP Publishing LLC.

These results are interpreted in Ref. 62 by two mechanisms that may act in parallel and contribute to the indentation-driven voltage shift of the Q-V hysteresis loops: i) defect-dipole realignment and concurrent space charge rearrangement, and ii) reduction of the clamping effect on domains controlled by a variation of the internal residual stress. The later mechanism results in the enhanced polarization state of the film, the so-called interfacial poling, and potentially may lead to more space charge trapping at the bottom electrode due to liberation of defect-stabilized domain walls. Koval *et al.* in their early work [63] reported on an increase of the effective piezoelectric coefficient upon nanoindentation in the PZT film capacitors and attributed it to the stress-enhanced irreversible movement of ferroelastic domain walls. This scenario is consistent with the theoretical and experimental works of other researchers.[64, 65] Pertsev and Emelyanov [66] have shown that the residual stresses can change significantly when a 90^0 domain wall is shifted from its equilibrium position by an external field.

Stress-driven effects in ferroelectric thin films indicate that reliability, performance and lifetime of ferroelectric capacitors can be significantly affected by mechanical force. Gruverman *et al.*

[67] have reported on the stress-induced poling and imprinting of (111)-oriented PZT-based capacitors. By using piezoresponse force microscopy (PFM) they observed that the application of either compressive or tensile stress can change the in-plane polarization component of the film via the flexoelectric effect, and thus produce FeRAM (Ferroelectric Random Access Memory) capacitors in a heavily imprinted state characterized by a strongly shifted hysteresis loop (Fig. 11). Recently, the possibility to write ferroelectric memory bits using pure mechanical force instead of electrical voltage in data storage devices has been proposed by Lu *et al.* [68].

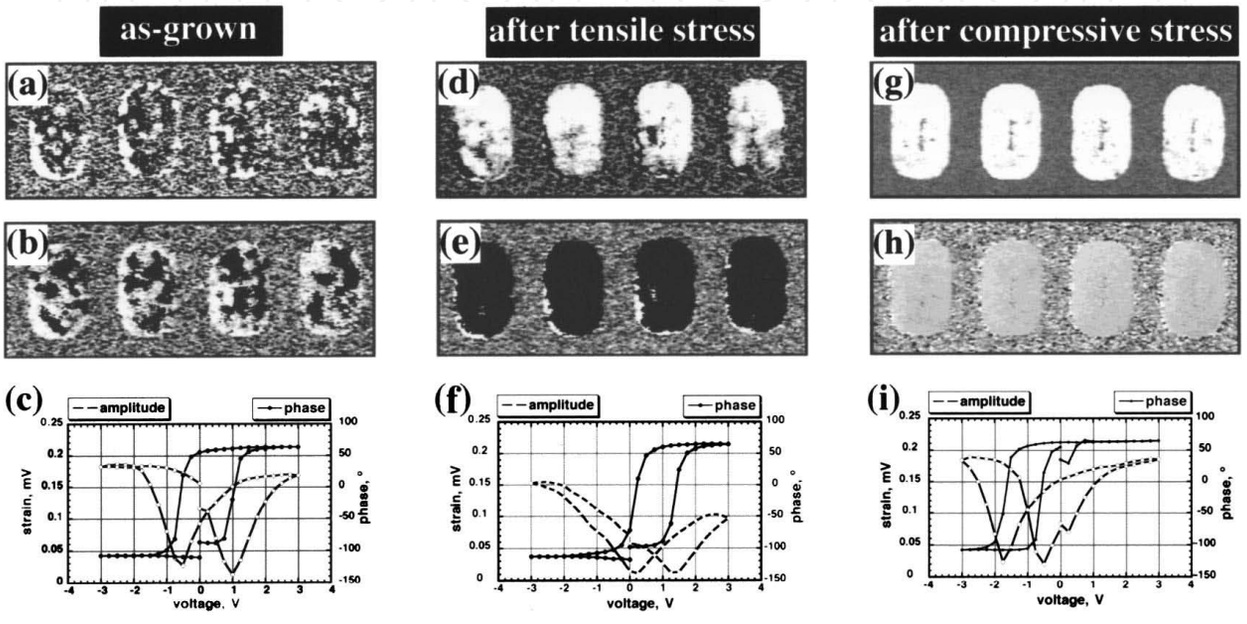

Figure 11. Stress-induced polarization reversal and switching characteristics of the (111)-oriented PZT capacitors. (a), (d) and (e) PFM amplitude images; (b), (e) and (h) PFM phase images; (c), (f) and (i) local hysteresis loops measured for as-grown capacitor, after tensile and compressive stress application, respectively. Reproduced with permission from Gruverman *et al*. [67]. Copyright 2003, AIP Publishing LLC.

3. Ferroelastic materials

3.1. Hysteresis and biasing effects in ferroelastic materials

Ferroelastic materials undergo a phase transition from a high temperature paraelastic phase to a low temperature ferroelastic phase at the Curie temperature, T_c. In the ferroelastic phase, there are two or more equilibrium and switchable orientation states, characterized by a different spontaneous strain. A shift from one state to another can occur during the application of a mechanical stress, and in most cases it gives rise to hysteretic stress-strain curves (Fig. 12).[69] In tension-compression loading, the stress at which the strain is zero is called *the coercive stress* (Fig. 12a). The intersection of the two branches of the hysteresis curve is defined as the "*critical stress*", where the system experiences significant changes in the domain pattern.

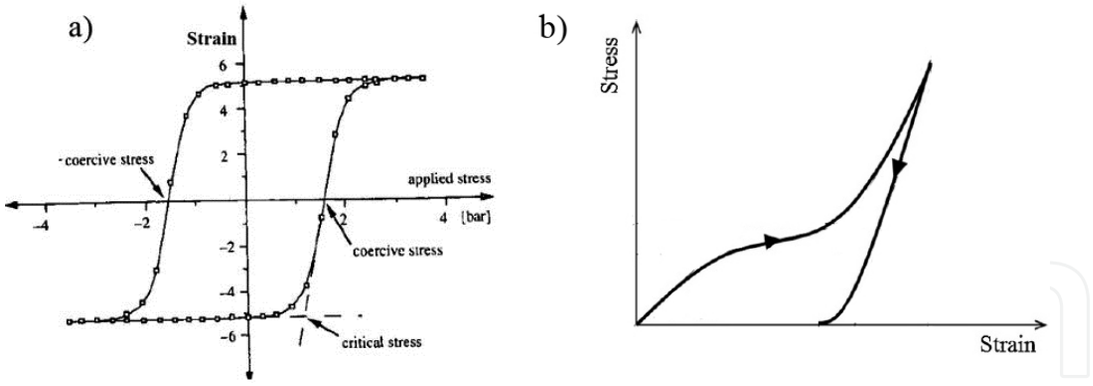

Figure 12. (a) Tension-compression stress-strain curve of a ferroelastic material. Reproduced with permission from Salje [67]. Copyright 1993, Cambridge University Press. (b) Compressive stress–strain curve of a ferroelastic material.

A number of complex oxides with a perovskite structure, and shape memory alloys exhibiting the martensitic transformation represent two important families of ferroelastic materials. In ferroelastic ceramics, it is difficult to generate the tension-compression hysteresis loops due to their brittleness, and thus ferroelasticity in these systems is preferably investigated by studying compression test curves.[70] A typical compressive stress–strain curve of a ferroelastic material is shown in Fig. 12b. At the beginning of loading, the strain increases almost linearly with stress. Above a critical stress, the stress-strain curve shows a clear nonlinearity due to ferroelastic domain switching. When most of the switchable domains have been reoriented, the strain will again increase linearly with the stress. The coercive stress is commonly identified with the stress corresponding to the minimum value of the local slope of the stress-strain curve. It should be mentioned that in polar ferroelastic systems, where the spontaneous strain reorientation is also accompanied by polarization changes, the mechanical response depends on the electrical boundary conditions. In particular, higher stiffness is usually observed in open circuit conditions.

3.2. Perovskite oxides

Perovskite oxides may exhibit asymmetric deformation under external tensile and compressive mechanical loading. Fett *et al.* [71] performed bending tests on unpoled and poled soft PZT ceramics and reported that in both cases the region of the samples under tension and compression exhibit different deformation behaviour (Fig. 13).

The compression stress-strain curves of soft and hard PZT ceramics show large differences. Acceptor-doped PZTs, which behave as "hard" ferroelectrics, present an analogous "hard" behaviour under mechanical loading, characterized by a low elastic compliance, a high coercive stress and a large mechanical factor of quality. Cao *et al.* [72] systematically studied the strain and polarization variations of soft and hard PZT ceramics upon unipolar compressive stress cycles applied parallel and perpendicularly to the poling direction. They found that both hard and soft PZT exhibit a nonlinear stress-strain curve when the stress exceeds a critical value at which ferroelastic domain switching begins to occur (Fig. 14). From the figure, one can see that the coercive stress of hard PZT is larger than that of the soft composition. In

http://dx.doi.org/10.5772/60764

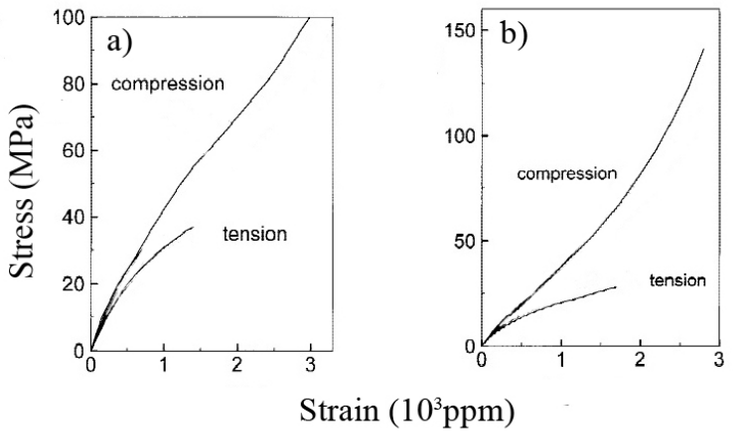

Figure 13. Stress–strain curves for the (a) unpoled and (b) poled PZT ceramics. After [71].

addition, hard PZT can recover most of their nonlinear strain upon unloading, whereas the nonlinear strain of soft PZT is mostly unrecoverable (Fig. 14a). Similar behaviour can be also observed in the stress-depolarization curves (Fig. 14b). It is generally accepted that the main variations of both strain and polarization in ferroelectric/ferroelastic materials under mechanical stress result from the switching of 90° domains. When the stress is perpendicular to the poling direction, the stress-strain curves show lower strain values (Fig. 14c) due to a smaller amount of domain reorientation compared to the parallel case. Hard PZT has a more stable domain structure and thus the strain and the polarization changes, induced by the applied mechanical stress, are smaller than those of the soft PZT ceramics (Fig. 14c). Marsilius *et al.* [73] studied the stress-strain behaviour of the soft and hard ferroelectric/ferroelastic ceramics at different temperatures and found that hard ceramics have a larger coercive stress and a larger coercive field than soft ceramics. In addition, they demonstrated that the difference between the coercive mechanical stresses of soft and hard materials is much larger than the difference between their coercive electric fields. This suggests that the effect of doping on stress-induced ferroelastic switching is greater than the effect of doping on the domain switching induced by an external electrical field. For mechanical stresses above 200 MPa, both the soft and hard ceramics showed similar mechanical behaviour, indicating that above a certain threshold the hardening mechanisms of doping can be eliminated by the switching of the defect dipoles in the direction perpendicular to the loading direction. Similar hardening effects were also observed in the ferroelastic non-polar $LaCoO_3$ ceramics after a partial substitution of La with the acceptor ions of Ca, which determined a suppression of domain wall movement within the sub-coercive stress region [74] and an increase of the coercive stress [75].

Picht *et al.* [76] measured the stress-strain curves of unpoled $BaTiO_3$ in short circuit conditions at different temperatures. As shown in Fig. 15, at room temperature $BaTiO_3$ displays a compressive stress-strain curve typical of a ferroelastic material. The remanent strain and the hysteresis area decrease with increasing temperature. When the stress-strain curves were measured at the Curie point (T = 127 °C) and at a slightly higher temperature (e.g., T = 130 °C), a double stress-strain loop was observed (Fig. 15). The hysteresis disappeared when the

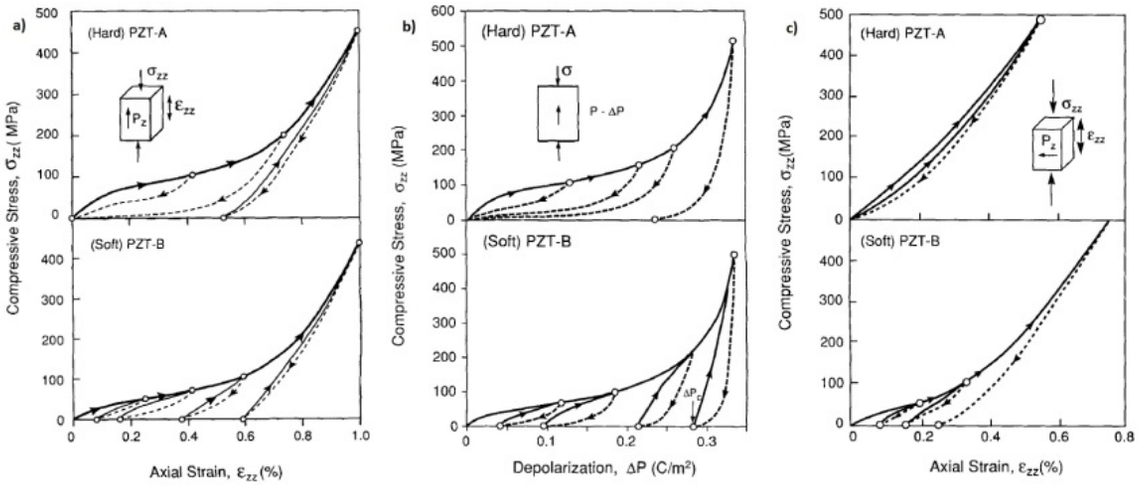

Figure 14. (a) Stress-strain curves of the soft and hard PZT ceramics under compression with the applied stress parallel to the polarization. (b) Depolarization vs. compressive stress curves of the hard and soft PZT ceramics. (c) Stress-strain curves of the soft and hard PZT ceramics under compression with the stress applied perpendicular to the polarization. Reproduced with permission from Cao and Evans [72]. Copyright 1993, Willey & Sons, Inc.

temperature was increased above 138 °C. The presence of the double loop above the Curie point was ascribed to a stress-induced paraelastic-to-ferroelastic phase transition.

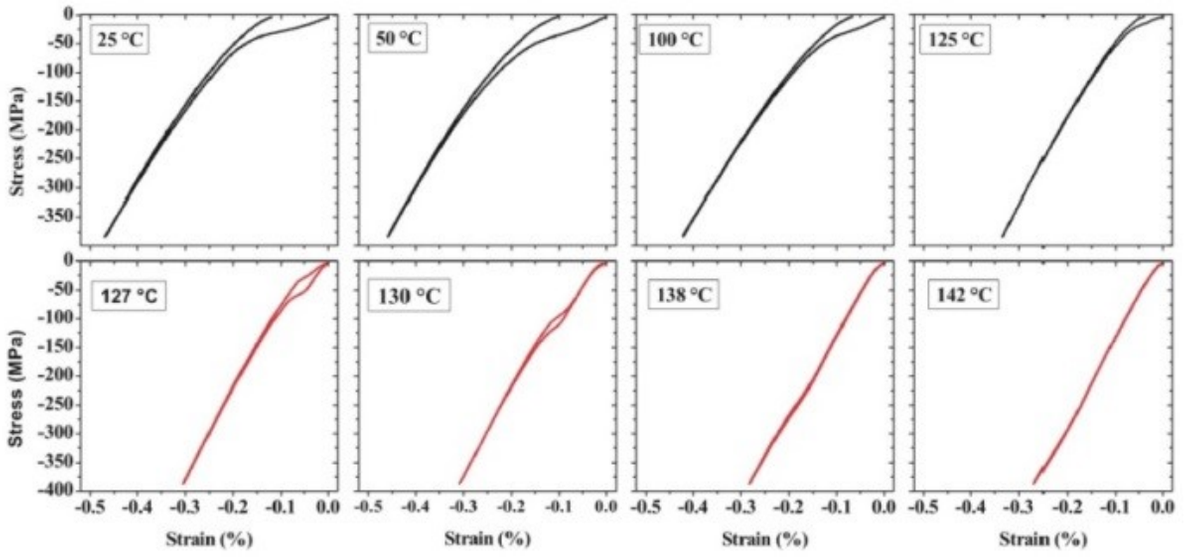

Figure 15. Stress-strain curves of $BaTiO_3$ ceramics at different temperatures. Reproduced with permission from Picht *et al*. [76]. Copyright 2012, AIP Publishing LLC.

3.3. Shape memory alloys

Shape memory effect refers to a shape recovery of ferroelastics during heating at high temperatures after a deformation process induced at a lower temperature. The most important class of materials exhibiting a strong shape memory effect is represented by Shape Memory

http://dx.doi.org/10.5772/60764

Alloys (SMAs). Plietsch *et al.* [77] have studied the stress-strain curves of the NiTi alloys subjected to either tension or compressive stress at different temperatures. They found that the pseudoelastic and martensitic NiTi phases show a pronounced asymmetry in stress-strain behaviour (Fig. 16). The asymmetry in the martensitic phase was ascribed to the different strength under tension and compression, which is likely caused by the presence of internal cracks, residual stresses or due to the Bauschinger effect.

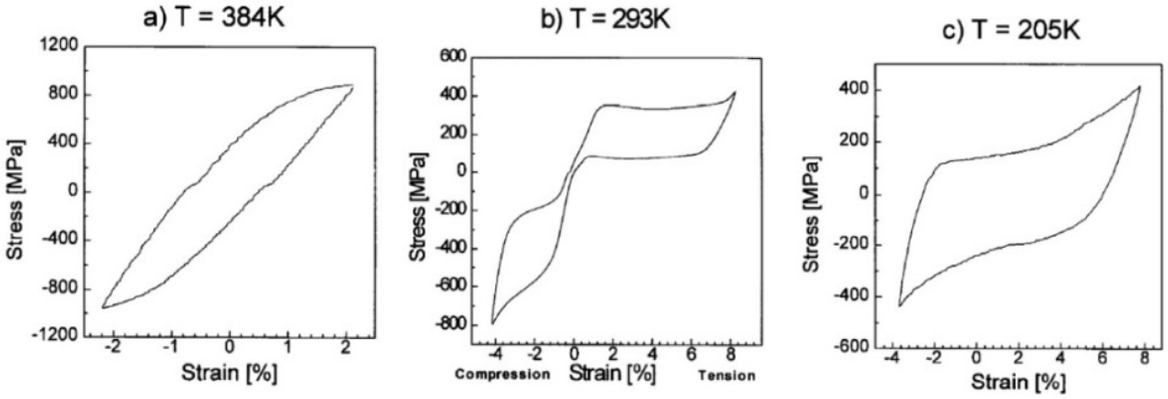

Figure 16. Tension/compression hysteresis for NiTi: (a) austenitic, (b) pseudoelastic, and (c) martensitic alloy. These images were published in Plietsch and Ehrlich [77]. Copyright 1997, Elsevier.

Liu *et al.* [78] have systematically studied tension-compression behaviour of martensitic NiTi under both monotonic and cyclic tensile/compressive loading. They found that the deformation mechanisms of the martensite phase are different under tension and compression, as evidenced by the asymmetric stress-strain curves (Fig. 17). Transmission electron microscopy (TEM) observations revealed that in the non-deformed specimen the martensite variants are well self-accommodated through the martensite twinning. Under tension, the interfaces between two variants are mobile and can migrate under stress. On the other hand, no migration of the junction planes between the neighbouring martensite plates was observed in samples compressed up to 4% strain. Instead, a high density of lattice defects, mainly dislocations, was observed inside both the martensite twin bands and twin boundaries. It was suggested that in the martensite phase the deformation mechanism under tension up to 4% may be predominantly related to the migration of variant interfaces, while under compression up to 4%, the strain is likely caused by the generation and movement of lattice defects, mostly dislocations.

3.4. The Bauschinger effect

The Bauschinger effect refers to the phenomenon by which the yield stress of metals reduces in the direction opposite to that of the very first stress applied.[79] This effect is believed to play a dominant role in the asymmetrical strain-stress behaviour of both monotonically and cyclic deformed metals. The effect is closely related to the presence of a long range internal stress (LRIS). The concept of LRIS assumes that the variations of the local stresses due to the

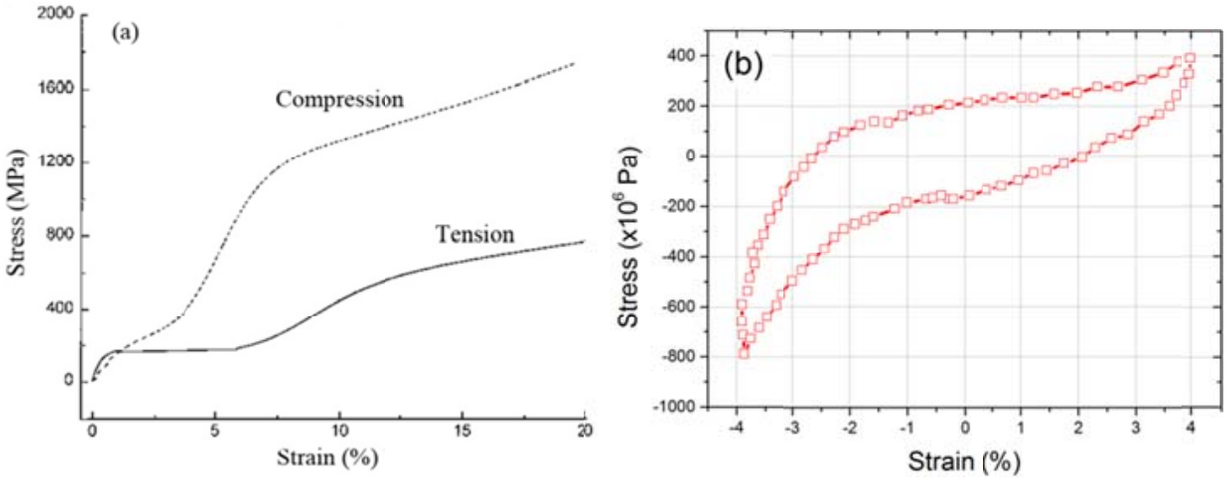

Figure 17. Stress-strain curves of a NiTi SMAs under (a) a monotonic tension and compression and (b) tension-compression cyclic loading within 4% strain. After [78].

applied stress occur over the long length scales. After plastic deformation have been produced, high dislocation density regions, such as sub-grain boundaries, and low dislocation density regions, such as cell interiors, characterized by a different yield stress are formed in the system. Under mechanical loading, the internal stress of the high-dislocation density regions is higher than that in low-dislocation density regions. Upon unloading, the average internal stress is zero; at the same time, the stress in the high dislocation density regions is positive, while it is negative in the low dislocation density regions. As a consequence, during stress reversal (applied stress changes sign), plasticity occurs in the low dislocation density regions at a lower stress and gives rise to the observed lower yield stress.

3.5. Microscopic mechanisms

In SMAs, the defects that might be present in the system, such as vacancies and solute atoms, tend to distribute following a short-range order symmetry, which will comply with the crystal symmetry after aging treatments.[80] In the aged martensite (Fig. 18a), the short-range order symmetry of defects conforms with the crystal symmetry of the martensite phase. During heating, the short-range ordering of defects does not change abruptly into a cubic symmetry at temperatures above the diffusionless martensitic transformation, because the diffusion of defects is a slow process (Fig. 18b). After aging, the short-range order symmetry of defects becomes conformed to the cubic crystal symmetry of the austenite parent phase (Fig. 18c). This phenomenon is referred to as the symmetry-conforming property of point defects in ferroelastic systems.[80] It should be mentioned that the short-range order of defects with martensitic symmetry can slightly distort the cubic lattice towards the martensitic symmetry, when the martensite is quickly heated up to the cubic phase. Such a lattice difference will produce a short range order-induced domain pattern in the cubic phase identical to the martensitic domain pattern. Thus, the symmetry property of point defects can give rise to the aging-induced two-way shape memory effect, namely the one observed in the aged martensitic phase of $Au_{51}Cd_{49}$ SMA.[80]

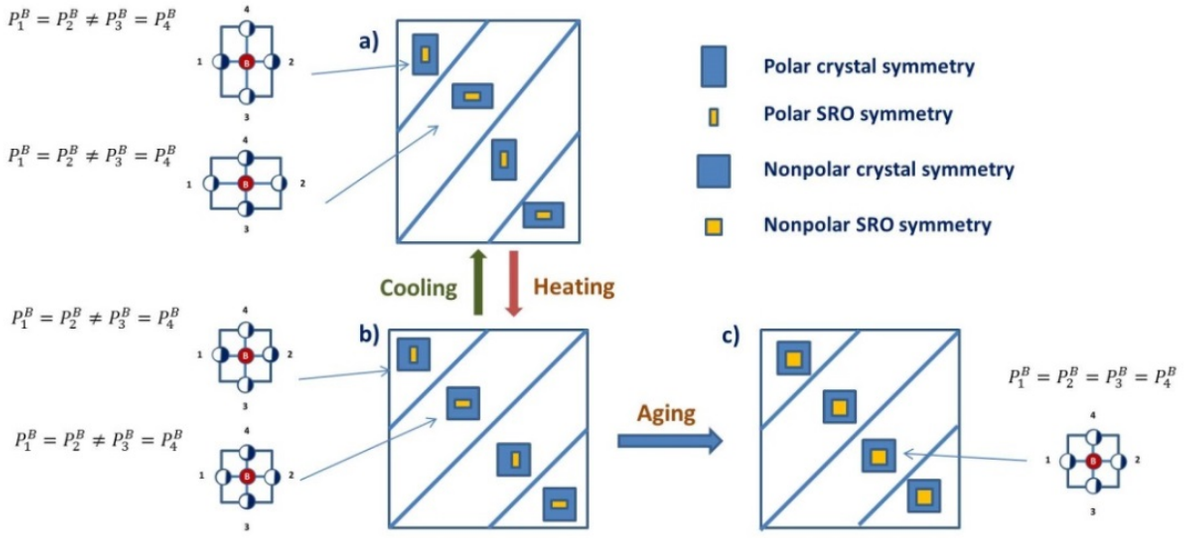

Figure 18. Predicted microstructure and short range order changes during reverse martensitic transformation from symmetry conforming short range order principle. (a) Aged martensite in which short range order symmetry conforms to the crystal symmetry of martensite. (b) Parent phase immediately after diffusionless transformation from (a). (c) Parent phase after aging that allows for the short range order symmetry of defects to conform to the cubic symmetry of the parent phase. After [80].

4. Ferromagnetic materials

4.1. Distortions of M-H hysteresis loops

In ferromagnetic materials, there is an intense direct exchange interaction between the magnetic moments of adjacent atoms due to the overlapping of atomic orbitals. The spins tend to align parallel each other and induce a spontaneous magnetization. The application of an alternating magnetic field produces a hysteretic magnetization-magnetic field (M-H) loop (Fig. 19). During the application of the very first magnetic field cycle, the ferromagnetic material becomes magnetized to the saturated state with a saturated magnetization (M_s). By decreasing the magnetic field to zero, the magnetization decreases and shows a remanent magnetization (M_r) at zero field. The magnetic field corresponding to zero magnetization represents the coercive magnetic field (H_c).

In absence of biasing effects, the M-H hysteresis loops of ferromagnetic materials display certain symmetry characteristics with respect to both H- and M-axis. However, these can be lost consequently to the development of different type of biasing processes that give rise to the deformed and shifted M-H loops along both axes. In this context, two main mechanisms will be discussed; the *exchange bias effect* and the *coexistence of amorphous and crystalline phases.*

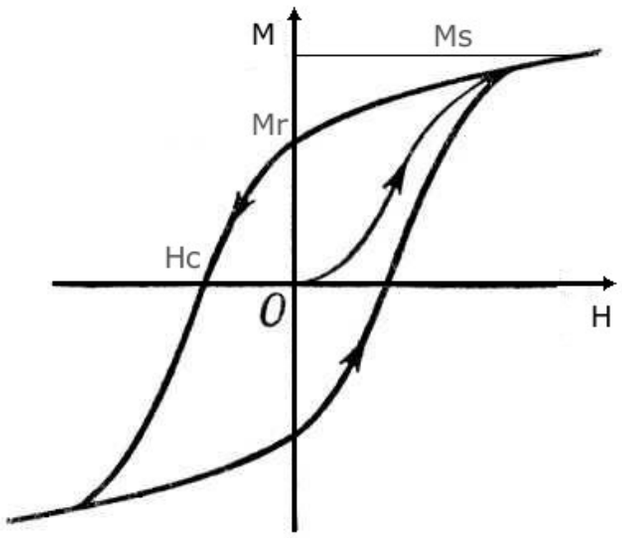

Figure 19. Magnetic M-H hysteresis loops of a ferromagnetic.

4.2. Exchange bias effect

4.2.1. Shift of the M-H loop along the magnetic field axis

The exchange bias effect can be observed in systems containing interfaces between a ferromagnetic (FM) and an antiferromagnetic (AFM) phase, in which the Curie temperature (T_c) of the FM is higher than the Neel temperature (T_N) of the AFM.[81] When the FM-AFM system is cooled through the T_N during the application of an external magnetic field (referred to as the cooling field H_{cf}), a shift of the M-H hysteresis loop of the FM-AFM system along the magnetic field axis may appear. This defines the exchange bias field (H_E).[82] The exchange bias phenomenon was firstly discovered by Meiklejohn and Bean in Co (ferromagnetic)-CoO (antiferromagnetic) system.[83] Later, the exchange bias has been observed in many other systems, including nanoparticles, inhomogeneous materials, single crystals and thin films containing FM-AFM, ferrimagnetic-FM and ferrimagnetic-AFM interfaces. The first intuitive mechanism proposed by Nogues *et al.* [84] to explain the exchange bias effect is schematically drawn in Fig. 20. In the range $T_N < T < T_C$, the cooling field induces the alignment of the FM spins along its direction (Fig. 20i), while at $T < T_N$, the spins of the AFM phase arrange in an antiferromagnetic configuration (Fig. 20ii). Along the FM-AFM interface, the AFM spins tend to align ferromagnetically as they are influenced by those of the FM due to the FM exchange interaction (Fig. 20ii). When the magnetic field is reversed, the FM spins tend to reorient following the applied field, while the AFM spins remain unchanged due to the large AFM anisotropy (Figs. 20iii - 20v). The ferromagnetic interaction at the FM-AFM interface provides a strong restoring force on the FM spins reorientations, and thus a shift of the M-H loop is produced. Generally, when the interaction at the interface is ferromagnetic and the cooling field H_{cf} is applied along the positive direction, the exchange bias field H_E is characterized as a negative exchange bias field and a shift of the M-H loop towards the negative direction is observed (Fig. 20).

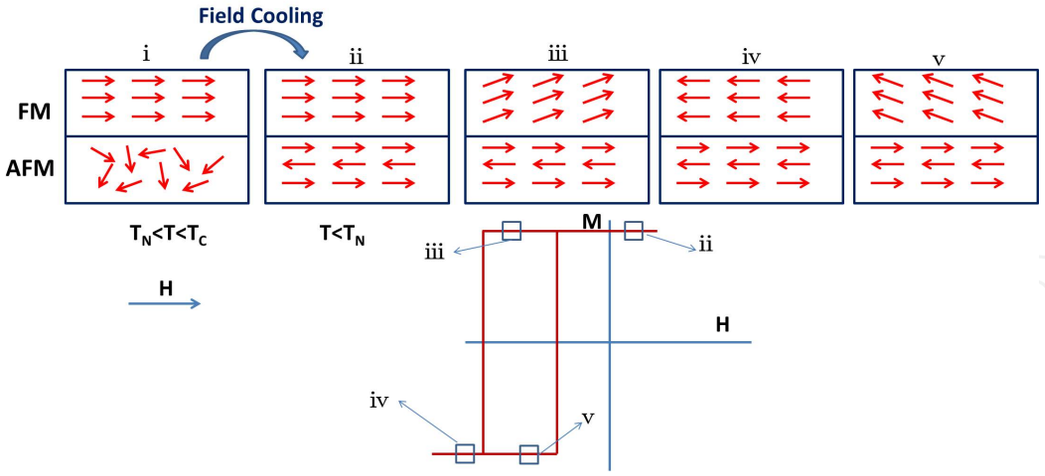

Figure 20. Schematic of the exchange bias mechanisms in case of ferromagnetic interaction between the FM and AFM spins at the interface. After [82].

However, it has been also understood that in some magnetic systems the interaction between the spins at the interfaces can be antiferromagnetic, meaning that below T_N the AFM spins in the layer close to the interface are aligned antiparallel to the FM spins. In this case, the direction of the M-H loop shift depends on the strength of the cooling field. Nogues *et al.* [84] have found that in Fe (FM)-FeF_2 (AFM) bilayers, the M-H hysteresis loops can shift along the direction of the cooling field, after a sufficiently large cooling field is applied (Fig. 21). It was proposed that in case of the antiferromagnetic interaction, when the system is cooled through T_N, the spins of AFM at the interface tend to align antiparallel to those of FM. By applying a low cooling field along the positive direction, the FM spins will align along the positive direction, while the AFM spins will not switch. When the applied magnetic field is reversed, the FM spins will try to follow the field, while the AFM spins will oppose to that, and they will force the FM spins to be antiparallel to them, leading to a shift of the M-H loop towards left. However, when the positive cooling field is large enough, the AFM surface spins are forced to be parallel to the FM spins along the cooling field direction, and a positive exchange bias is developed. Therefore, when the applied field is reversed, the magnetization reversal is facilitated by the antiferromagnetic coupling of the spins at the interface, and a positive shift of the M-H loop is observed (Fig. 21).

In order to quantitatively describe the exchange bias effect, several phenomenological models have been proposed. The model developed by Meiklejohn [83] assumes that both the FM and the AFM are in single domain state, the FM-AFM interface is perfectly smooth, and the energy per unit interface area can be expressed as:

$$E = -HM_{FM}t_{FM}\cos(\theta-\beta) + K_{FM}t_{FM}sin^2(\beta) + K_{AFM}t_{AFM}sin^2(\alpha) - J_{INT}\cos(\beta-\alpha) \quad (8)$$

where H is the applied field, M_{FM} is the saturation magnetization, t_{FM} and t_{AFM} are the thickness of FM and AFM layers respectively, K_{FM} and K_{AFM} are the anisotropy of FM and AFM layers

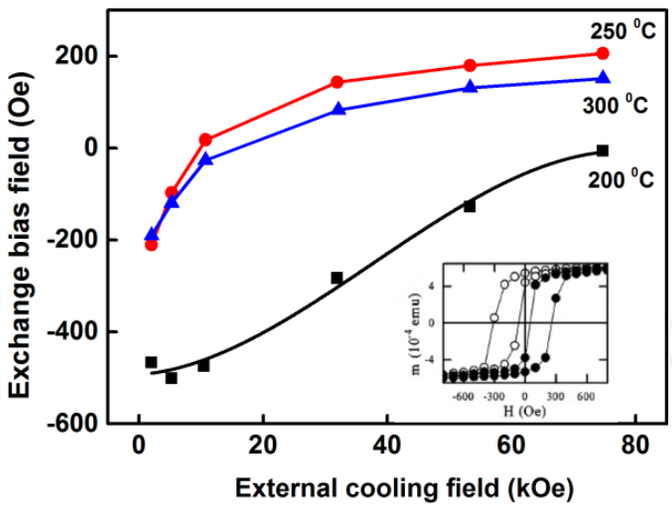

Figure 21. The exchange bias field as a function of the cooling field for FeF_2-Fe bilayers with the FeF_2 grown at different temperatures, square: 200°C, triangle: 250°C, and circle: 300°C. In-set: magnetization loops of the sample with FeF_2 grown at 300°C for low (hollow circle) and high (solid circle) cooling field. After [84].

respectively, and J_{INT} is the interface coupling constant. The terms α, β and θ represent the angles between K_{AFM} and M_{AFM}, $K_{FM,}$ and M_{FM}, K_{FM} and H, respectively.

By neglecting the FM anisotropy, which is much smaller than that of AFM, and by minimizing the energy with respect to α and β, the exchange bias is obtained as:

$$H_E = \frac{J_{INT}}{M_{FM} t_{FM}} \tag{9}$$

However, the exchange bias H_E calculated using the Eq. 9 is usually several orders of magnitude larger than the value observed in the experiments. Malozemoff [85] proposed an exchange bias effect model based on the assumption of rough FM-AFM interfaces. A microscopically random exchange field at the interface due to the defects, roughness or lattice mismatch can give rise to a random field which produces a number of uncompensated spins at the interface, leading to the loop shift. It was assumed that the FM is in a single domain state, therefore, due to the presence of a random field the AFM system will split into domains in order to minimize the unidirectional anisotropy (i.e., one single stable configuration of FM spins). The model gives the following expression for the exchange bias field [85]:

$$H_E = \frac{2z}{\pi^2 M_{FM} t_{FM}} \sqrt{\frac{J_{INT} K_{AF}}{a}} \tag{10}$$

where z is a constant in the order of unity related to the randomness degree of the interface and a is the lattice parameter of the FM lattice which was considered cubic. The exchange bias values estimated by this model are consistent with the experiments. However, the main

drawback of the model is that the calculated bias depends on the defect concentration at the interface. Mauri *et. al.* [86] developed a model assuming that the domain walls develop in the AFM layer, which sets an upper limit on the exchange coupling energy in such a manner that it ultimately gives rise to a significantly smaller exchange bias than that provided by the Meiklejohn's model calculations [83]. Using a micromagnetic approach, Koon [87] has stated that the orientation of the FM spins should be perpendicular to the AFM magnetic easy axes in the ground state. Although this model can explain the coercivity enhancement in some systems, it fails to provide reasonable estimations of the exchange bias. Therefore, the development of more general models to more accurately quantify the exchange bias in different systems is still ongoing.

Another kind of asymmetry characterized by a sharp step in the upper branch of the hysteresis loop was reported in the exchange biased Co-CoO dot array system.[88] The hysteresis loops of the Co-CoO dot arrays with four different dot sizes are shown in Fig. 22. Together with a shift of the hysteresis loops along the H-axis due to the exchange bias, a peculiar anomaly can be observed in the upper branch of the M-H hysteresis loop. This loop distortion is considered to originate from the presence of an intermediate magnetization saturated state. Both loop features showed a strong dependence on the size of dots. The H-shift of the M-H loop reduces with decreasing the dot size due to a reduction of the exchange bias effect. The deformation in the upper branch of the M-H loop was attributed to a magnetostatic interaction between the dots. The interaction determines an intermediate saturation of the magnetization (indicated in Fig. 22 by an arrow), which hinders the magnetization reversal and lowers its rate. The stability of the intermediate magnetization is larger in the array with bigger dots (compare Figs. 22a-d). For the dots with smaller size, the inter-dot magnetostatic interaction is weaker and the magnetization switching of each dot is less influenced by those of the surrounding dots. This determines a faster magnetization switching rate and an almost complete disappearance of the intermediate saturation magnetization (Fig. 22d).

4.2.2. Shift of the M-H loop along the magnetization axis

In some magnetic systems containing the FM-AFM interfaces, the M-H hysteresis loop can also shift along the magnetization axis. Generally, the M-shift of the M-H loop is caused by the presence of a pinned magnetization which cannot be switched by the applied external magnetic field. The pinned magnetization can be developed through different mechanisms, including: i) an incomplete spin reversal of the FM spins; ii) the presence of spin glass-like phases in FM material nearby the interface region; iii) the presence of uncompensated spins in the AFM layer, and iv) the spin canting in the AFM layer. An example of systems where a spin glass-like arrangement develops in the FM phase is represented by the composite made up of granular ferrimagnetic $NiFe_2O_4$ nanoparticles embedded in an antiferromagnetic NiO matrix.[89] Fig. 23a shows the M-H hysteresis loops of the system measured at 10 K after both the zero-field cooling (ZFC) and field cooling (FC) processes. In the latter process, the M-H hysteresis loop shows a field offset as well as a magnetization shift with the exchange bias linearly increasing with the vertical magnetization offset. The underlying mechanism of the switching asymmetry in these materials was suggested to originate from the spin glass-like

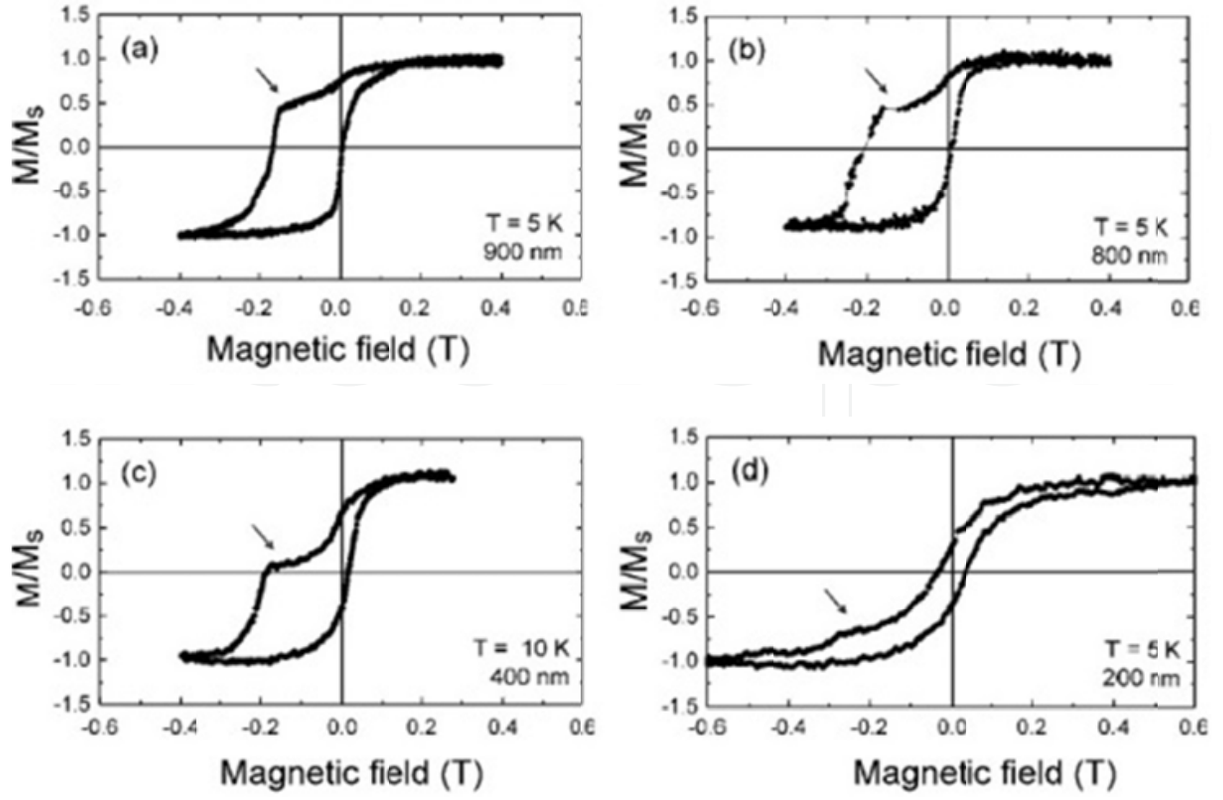

Figure 22. Hysteresis loops of the Co-CoO square dot arrays with four different dot sizes. Reproduced with permission from Girgis *et al*. [88]. Copyright 2003, APS.

phase formed in $NiFe_2O_4$ due to the fine particle size and the consequent structural disorder at the interface regions. During cooling under a magnetic field in the temperature range $T_{irr} < T < T_C$ (T_{irr} is the temperature above which the exchange bias disappears), the FM spins align along the applied magnetic field, while the spins of the glass-like phase remain randomly oriented. As the temperature is lowered below T_{irr}, some of the net uncompensated spins of the glass-like phase also line-up along the field-cooling direction and produce a pinned magnetization state. During the field reversal, the latter does not follow the field, which is probably the reason for the vertical shift of the loop. At the same time, the frozen spins in the glass-like phase try to keep the spins of the ferrimagnetic $NiFe_2O_4$ along their original direction leading to a negative shift of M-H loop along the H-axis.

The vertical shift of M-H hysteresis loops due to spin canting in the AFM layer was reported by Yuan *et al*. [90] for the $Co/Ca_2Ru_{0.98}Fe_{0.02}FeO_4$ (FM/AFM) heterostructure, where the Co layer was sputtered on the $Ca_2Ru_{0.98}Fe_{0.02}FeO_4$ single crystal. When the FM/AFM system was cooled down to 10 K in a magnetic field, a horizontal and a vertical shift of the M-H loop was observed. In particular, the shift along the H-axis is negative for a positive cooling field and positive for a negative cooling field. On the other hand, the shift along the M-axis is positive for a positive cooling field and negative for a negative cooling field (Fig. 23b). The $Ca_2Ru_{0.98}Fe_{0.02}FeO_4$ single crystal does not have uncompensated AFM spins, however, the magnetic moments of the Ru (Fe) ions in the B-site of the AFM oxide are canted and give rise to the net ferromagnetic

http://dx.doi.org/10.5772/60764

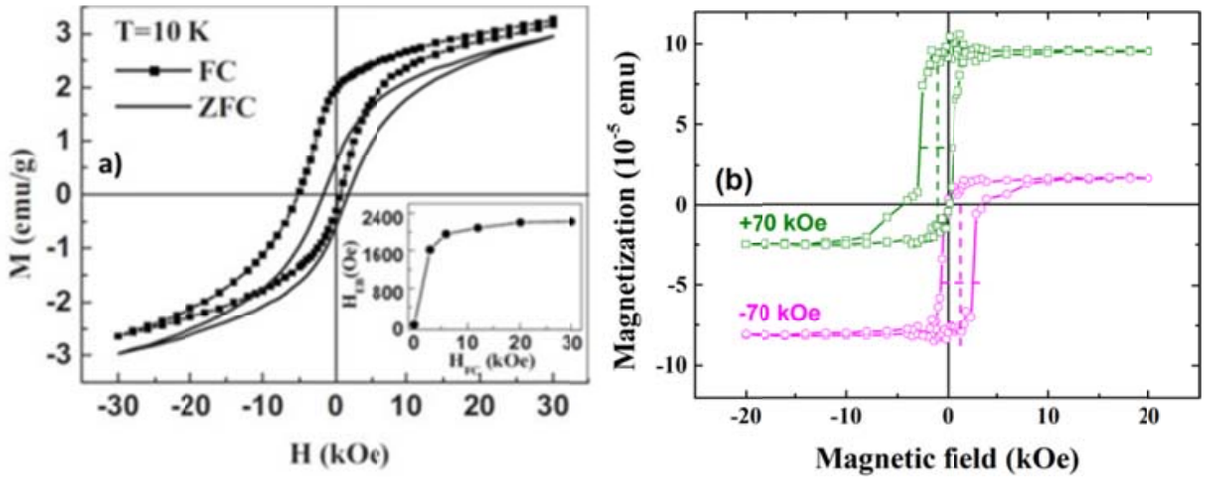

Figure 23. (a) The M-H hysteresis loops of $NiFe_2O_4$ nanoparticles embedded in an antiferromagnetic NiO matrix measured at 10 K. Reproduced with permission from Tian *et al*. [89]. Copyright 2008, AIP Publishing LLC. (b) The M-H hysteresis loops of $Co/Ca_2Ru_{0.98}Fe_{0.02}FeO_4$ heterostructure. Courtesy of S. J. Yuan, after [90].

moments. In the first layer near the Co phase, these moments align parallel to those of the Co layer, but they cannot be readily switched when the magnetic field is reversed. As a consequence, the vertical shift of the M-H hysteresis loops is produced (Fig. 23b). Nogues *et al.* [91] studied the dependence of the exchange bias and magnetization shift on cooling field in the Fe-FeF_2-Al system. They observed that for low cooling fields the vertical shift can be opposite to the cooling field suggesting that an antiferromagnetic coupling exists at the FM-AFM interface. Additionally, at low cooling fields, the vertical shift was negative when the thickness of the FeF_2 layer was 200 nm and it was positive for the 100 nm layer. This behaviour was attributed to the roughness of the interface; smooth interface tends to induce a negative vertical shift, while rough interface usually leads to a positive shift. For large cooling fields, a positive vertical shift was observed in all cases.

The vertical offsets of M-H hysteresis loops were also observed in magnetic systems without exchange bias. Watanabe *et al.* [92] reported on the shift of the magnetization hysteresis loop along the magnetization axis in the antiferromagnetic $LaFeO_3$ when cooled in a magnetic field below the Neél temperature. The shift phenomenon was explained by the fact that the field-cooled $LaFeO_3$ always shows a weak ferromagnetism with a small remanent magnetization, which cannot be reversed by the external field. A vertically shifted M-H hysteresis loop was also observed in Co_2VO_4 at 4.2 K when cooled in a small magnetic field.[93] Due to the high anisotropy and magnetic hardness of cobalt in spinel lattices, the spins of cobalt ions align along the cooling field direction when cooled through the Curie temperature and, at low temperatures, they preserve the orientation producing the shift of M-H loop along the magnetization axis.

4.3. Effect of the amorphous-crystalline phases coexistence

A distinct shift of the M-H hysteresis loop was observed in magnetic systems subjected to a conventional annealing at a temperature below their crystallization temperature. Ohta *et al.*

[94] studied the $Fe_5Co_{70}Si_{10}B_{15}$ amorphous alloys and reported that the as-quenched sample shows a symmetric hysteresis loop (Fig. 24a). After annealing at 420 °C, the hysteresis loop becomes pinched (Fig. 24b) and annealing under a magnetic field of 10 kOe leads to a significant shift of the loop along the H-axis (Fig. 24c).

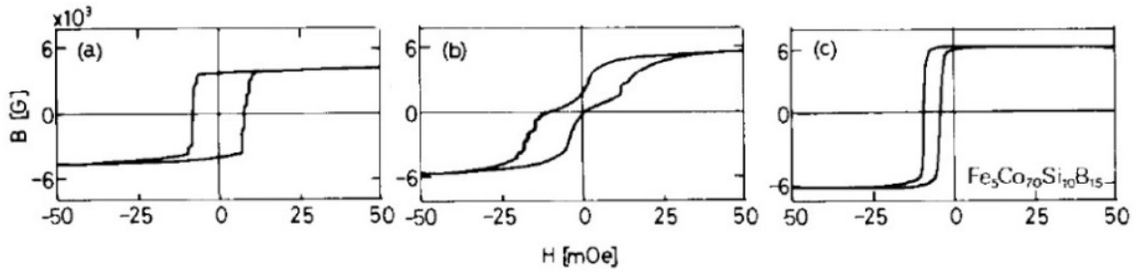

Figure 24. The magnetic induction (B) vs. magnetic field (H) hysteresis loops of amorphous alloys $Fe_5Co_{70}Si_{10}B_{15}$: (a) as-quenched, (b) annealed and (c) annealed in a magnetic field. These images were published in Ohta *et al*. [94]. Copyright 1980, Elsevier.

Kohmoto *et al.* [95] have reported on the loop shift of the $Fe_5Co_{70}Si_{10}B_{15}$ amorphous alloys annealed at 180 °C for different time. The shift along the field axis was found to increase with the increase of annealing time. Rivas *et al.* [96] observed the shifted M-H loops in the metallic-glass $Co_{66}Si_{16}B_{12}Fe_4Mo_2$ ribbons annealed at 510 °C and "pre-magnetized" under a magnetic field of 400 kA/m at room temperature. A large negative field offset was observed when the initial applied field was parallel to the pre-magnetizing field, and the field shift was positive as the initial applied field was antiparallel to the pre-magnetizing field. However, no shift of M-H hysteresis loops was observed when the magnetic field was applied perpendicular to the direction of the pre-magnetizing field. The results suggest that the shift of M-H hysteresis loops in the annealed pre-magnetized ribbons originate from the coexistence of the amorphous and crystalline phases. After annealing, the amorphous matrix contains partially crystallized particles which are much magnetically harder if compared to the amorphous matrix. When subjected to a relatively high pre-magnetizing field, the magnetic moments of the particles tend to align along the applied field direction. Due to the large magnetic anisotropy, the magnetic spins of the hard-magnetic particles remain unchanged under the ac applied magnetic field used for the reorientation of the magnetic moments in the soft matrix. Therefore, a strong unidirectional dipolar magnetic field is formed, which can exert a strong restoring force on the reorientations of magnetic moments of the soft matrix, and thus produces a shift of M-H hysteresis loops.

4.4. Magnetic aging

The term "magnetic aging" indicates the time-dependent changes in the magnetization of ferromagnetic materials. These changes are also commonly referred to as "magnetic viscosity" or "magnetic after-effects". The typical relaxation time spans several orders of magnitude; it ranges from less than a second in superparamagnetic particles to millions of years in magnetic rocks.[97] Various mechanisms that contribute to the magnetic aging have been proposed,

including i) thermal fluctuations, ii) the diffusion after-effect of ferrous ions and vacancies, iii) chemical modifications.[98] The magnetic aging originated from thermal fluctuations is driven by the thermally activated jumps over energy barriers of domain walls. This process determines the time-, temperature- and magnetic field-dependence of the remanent magnetization. The diffusion of point defects, impurity atoms or electrons towards domain walls can cause the departure of the domain wall energy from a minimum which determines the displacement of the domain walls in a new equilibrium configuration. This type of magnetic aging mechanism is usually defined as "diffusion after-effect". It was first observed in iron containing carbon or nitrogen impurities.[98]

5. Summary

Biasing effects in different ferroic systems show a highly complex phenomenology which depends on several variables whose significance and contribution vary from case to case. Biased P-E and S-E ferroelectric loops are mainly generated by aging and fatigue processes, which are generally caused by the arrangement of charged defects and charge carriers in a certain configuration. A common cause of these two processes can be attributed to the development of an internal bias, which induces preferential polarization and strain configurations. In aging, the presence of an internal bias gives rise to pinched and asymmetric/shifted loops, while in fatigued samples the bias results in asymmetric and shifted loops. These features are mostly reversible upon opportune thermal treatments or electrical cycling, but fatigue shows also irreversible effects consisting, for instance, of mechanical damage such as microcracks that cannot be recovered. Aging effects are homogeneous since the controlling mechanisms are active down to the unit cell scale according to the symmetry-conforming property of point defects. Fatigue features instead can be highly inhomogeneous due to the screening retardation of the locally varying depolarizing field during electric field cycles. Under certain circumstances, aging of ferroelectrics can be explained within the concept of the symmetry-conforming property of point defects, which seems to be able to satisfactorily explain also biasing effects in non-polar ferroelastic materials. According to this principle, short-range ordered defects in ferroelastics tend to arrange themselves over time following the crystal symmetry of the hosting unit cell. The time-dependent change in the symmetry of point defects induces memory effects of equilibrium configurations, determining biased stress-strain hysteresis loops. In ferroelectric/ferroelasic perovskites, a partial replacement of A- and B-site cations with acceptor and donor species, respectively, produces analogous hardening and softening effects on ferroelectric and ferroelastic hysteresis loops under electric field and mechanical stress. Biasing effects in single phase ferromagnetic systems are usually generated by spatially inhomogeneous arrangement of spins on the unit cell scale. In magnetic heterostructures and composites characterized by the simultaneous existence of ferromagnetic and antiferromagnetic ordering within the material, biasing effects are due to the competitive contributions from the coexisting soft and hard magnetic phases. The exchange interaction at the interfaces between dissimilar phases, the presence of the uncompensated spins, the formation of spin glass-like phases and spin canting effects, together with pinned preferential

magnetization states are the most important possible mechanisms of biased M-H hysteresis loops. The thermally activated magnetic aging and the existence of domain wall pinning/depinning and rejuvenation effects in ferromagnetic materials introduce common characteristics with aging phenomena in ferroelectric/ferroelastic systems.

Acknowledgements

This work was done within the frame of the project no. 2/0057/14, which is supported by the Grant Agency of the Slovak Academy of Sciences.

Author details

Vladimir Koval[1*], Giuseppe Viola[2,3] and Yongqiang Tan[4]

*Address all correspondence to: vkoval@imr.saske.sk

1 Institute of Materials Research, Slovak Academy of Sciences, Kosice, Slovakia

2 Department of Applied Science and Technology, Institute of Materials Physics and Engineering, Torino, Italy

3 School of Engineering and Materials Science, Queen Mary University of London, London, UK

4 School of Physics, Shandong University, China

References

[1] Yan H, Inam F, Viola G, Ning H, Zhang H, Jiang Q, Zhang T, Gao Z, Reece MJ. The contribution of electrical conductivity, dielectric permittivity and domain switching in ferroelectric hysteresis loops. Journal of Advanced Dielectrics 2011;1(1) 107-118.

[2] Viola G, Saunders T, Wei X, Chong KB, Luo H, Reece MJ, Yan H. Contribution of piezoelectric effect, electrostriction and ferroelectric/ferroelastic switching to strain-electric field response of dielectrics. Journal of Advanced Dielectrics 2013;3(1) 1350007-11.

[3] Jin L, Li F, Zhang S. Decoding the Fingerprint of Ferroelectric Loops: Comprehension of the material properties and structures. Journal of American Ceramics Society 2014;97(1) 1–27.

[4] Genenko YA, Glaum J, Hoffmann MJ, Albe K. Mechanisms of aging and fatigue in ferroelectrics. Materials Science and Engineering B 2015;192 52-82.

[5] Tan Y, Zhang J, Wang C. Aging behaviours of CuO modified $BaTiO_3$ ceramics. Advances in Applied Ceramics 2014;113(4) 223-227.

[6] Arlt G, Neumann H. Internal bias in ferroelectric ceramics: Origin and time dependence. Ferroelectrics 1988;87(1) 109-120.

[7] Feng Z, Ren X. Striking similarity of ferroelectric aging effect in tetragonal, orthorhombic and rhombohedral crystal structures. Physical Review B 2008;77(13) 134115-6.

[8] Zhang L, Ren X. Aging behavior in single-domain Mn-doped BaTiO3 crystals: Implication for a unified microscopic explanation of ferroelectric aging. Physical Review B 2006;73(9) 094121-6.

[9] Tutuncu G, Damjanovic D, Chen J, Jones JL. Deaging and asymmetric energy landscapes in electrically biased ferroelectrics. Physical Review Letters 2012;108(17) 177601-5.

[10] Carl K, Hardtl KH. Electrical after-effects in Pb(Ti, Zr)O_3 ceramics. Ferroelectrics 1978;17(1) 413-486.

[11] Lupascu D, Genenko YA, Balke N. Aging in ferroelectrics. Journal of American Ceramic Society 2006;89(1) 224–229.

[12] Takahashi M. Space charge effect in lead zirconate titanate ceramics caused by the addition of impurities. Japan Journal of Applied Physics 1970;9(10) 1236-1246.

[13] Morozov MI, Damjanovic D. Charge migration in Pb(Zr, Ti)O_3 ceramics and its relation to ageing, hardening and softening. Journal of Applied Physics 2010;107(3) 034106-10.

[14] Tan Q, Li J, Viehland D. Role of lower valent substituent-oxygen vacancy complexes in polarization pinning in potassium-modified lead zirconate titanate. Applied Physics Letters 1999;75(3) 418-420.

[15] Balke N, Lupascu D, Granzow T, Rödel J. Fatigue of lead zirconate titanate ceramics. I: Unipolar and DC loading. Journal of American Ceramics Society 2007;90(4) 1081-1087.

[16] Luo Z, Glaum J, Granzow T, Jo W, Dittmer R, Hoffman M, Rödel J. Bipolar and unipolar fatigue of ferroelectric BNT-based lead-free piezoceramics. Journal of American Ceramics Society 2011;94(2) 529-535.

[17] Viola G, Tan Y, Saunders T, Reece MJ. Unpublished data.

[18] Jiang QY, Subbarao EC, Cross LE. Fatigue in PLZT: acoustic emission as a discriminator between microcracking and domain switching. Ferroelectrics 1994, 154(1) 113–118.

[19] Nuffer J, Lupascu D, Glazounov A, Kleebe HJ, Rödel J. Microstructural modifications of ferroelectric lead zirconate titanate ceramics due to bipolar electric fatigue. Journal of the European Ceramic Society 2002;22(13) 2133-2142.

[20] Priya S, Kim HW, Ryu J, Uchino K., Viehland D. Fractal cluster modeling of the fatigue behavior of lead zirconate titanate. Applied Physics Letters 2002;80(4) 1625-1627.

[21] Chen J, Harmer MP, Smyth DM. Compositional control of ferroelectric fatigue in perovskite ferroelectric ceramics and thin films. Journal of Applied Physics 1994;76(9) 5394-5398.

[22] Zuo R, Xu Z, Li L. Dielectric and piezoelectric properties of Fe_2O_3-doped $(Na_{0.5}K_{0.5})_{0.96}Li_{0.04}Nb_{0.86}Ta_{0.1}Sb_{0.04}O_3$ lead-free ceramics. Journal of Physics and Chemistry of Solids 2008;69(7) 1728-1732.

[23] Glaum J, Hoffman M. Electric Fatigue of Lead-Free Piezoelectric Materials. Journal of the American Ceramics Society 2014;97(3) 665-680.

[24] Viola G, Ning H, Reece MJ, Wilson R, Correia TM, Weaver P, Cain M, Yan H. Reversibility in electric field-induced transitions and energy storage properties of bismuth-based perovskite ceramics. Journal of Physics D: Applied Physics 2012;45(35) 355302-7.

[25] Viola G, Ning H, Wei X, Deluca M, Adomkevicius A, Khaliq J, Reece MJ, Yan H. Dielectric relaxation, lattice dynamics and polarization mechanisms in $Bi_{0.5}Na_{0.5}TiO_3$-based lead-free ceramics. Journal of Applied Physics 2013;114(1) 014107-9.

[26] Viola G, McKinnon R, Koval V, Adomkevicius A, Dunn S, Yan H. Lithium-induced phase transitions in lead-free $Bi_{0.5}Na_{0.5}TiO_3$ based ceramics. Journal of Physical Chemistry C 2014;118(16) 8564-8570.

[27] Luo Z, Granzow T, Glaum J, Jo W, Rödel J, Hoffman M. Effect of ferroelectric long-range order on the unipolar and bipolar electric fatigue in $Bi_{1/2}Na_{1/2}TiO_3$-based lead-free piezoceramics. Journal of the American Ceramics Society 2011;94(11) 3927-3933.

[28] Simons H, Glaum J, Daniels JE, Studer AJ, Liess A, Rödel J, Hoffman M. Domain fragmentation during cyclic fatigue in 94% $(Bi_{1/2}Na_{1/2})TiO_3$-6% $BaTiO_3$. Journal of Applied Physics 2012;112(4) 044101-5.

[29] Shur VY. Kinetics of polarization reversal in normal and relaxor ferroelectrics: relaxation effects. Phase Transitions 1998;65(1-4) 49-72.

[30] Balke N, Granzow T, Rödel J. Degradation of lead-zirconate-titanate ceramics under different dc loads. Journal of Applied Physics 2009;105(10) 104105-7.

[31] Shur VY, Nikolaeva EV, Shishkin EI, Baturin IS, Shur AG, Utschig T, Schlegel T, Lupascu D. Deaging in $Gd_2(MoO_4)_3$ by cyclic motion of a single planar domain wall. Journal of Applied Physics 2005;98(7) 074106-8.

[32] Shur VY, Rumyantsev EL, Nikolaeva EV, Shishkin EI, Baturin IS, Lupascu D, Nuffer J, Randall C, Ozgul M. Fatigue effect in bulk ferroelectrics. In: Lynch CS. (ed.) SPIE Proceedings on Smart Structures and Materials: Active Materials Structure and Mechanics 4699, July 15, 2002, San Diego, USA; 40-50. doi:10.1117/12.475015.

[33] Setter N, Damjanovic D, Eng L, Fox G, Gevorgian S, Hong S, Kingon A, Kohlstedt H, Park NY, Stephenson GB, Stolitchnov I, Taganstev AK, Taylor DV, Yamada T, Streiffer S. Ferroelectric thin films: Review of materials, properties, and applications. Journal of Applied Physics 2006;100(5) 051606.

[34] Ramesh R, Aggarwal S, Auciello O. Science and technology of ferroelectric films and heterostructures for non-volatile ferroelectric memories. Materials Science and Engineering: R: Reports 2001;32(6) 191-236.

[35] Koval V, Bharadwaja SSN, Trolier-McKinstry. Mist deposited lead zirconate titanate films. Ferroelectrics 2011;421(1) 23-29.

[36] Polcawich RG, Trolier-McKinstry S. Piezoelectric and dielectric realibility of lead zirconate titanate thin films. Journal of Materials Research 2000;15(1) 2505-2513.

[37] Warren WL, Tuttle BA, Dimos D, Pike GE, Al-Shareef HN, Ramesh R, Evans JT. Imprint in ferroelectric capacitors. Japanese Journal of Applied Physics 1996;35(2S) 1521-1524.

[38] Grossmann M, Lohse O, Bolten D, Boettger U, Schneller T. The interface screening model as origin of imprint in $PbZr_xTi_z$-xO_3 thin films. I. Dopant, illumination, and bias dependence. Journal of Applied Physics 2002;92(5) 2680-2687.

[39] Warren WL, Dimos D, Pike GE, Vanheusden K, Ramesh R.. Alignment of defect dipoles in polycrystalline ferroelectrics. Applied Physics Letters 1995;67(12) 1689-1691.

[40] Kim SH, Hong JG, Streiffer SK, Kingon AI. Imprint and fatigue properties of chemical solution derived $Pb_{1-x}La_x(Zr_yTi_{1-y})(1-x/4)O_3$ thin films. Journal of Materials Research 1999;14(4) 1371-1377.

[41] Folkman CM, Baek SH, Nelson CT, Jang HW, Tybell T, Pan XQ, Eom CB. Study of defect-dipoles in an epitaxial ferroelectric thin film. Applied Physics Letters 2010;96(5) 052903.

[42] Dimos D, Warren WL, Sinclair MB, Tuttle BA, Schwartz RW. Photoinduced hysteresis changes and optical storage in (Pb, La)(Zr, Ti)O_3 thin films and ceramics. Journal of Applied Physics1994;76(7) 4305-4315.

[43] Sze SM. Physics of Semiconductor Devices. Section 7.3.4, New York: Wiley&Sons; 1969.

[44] O'Dwyer J. The Theory of Dielectric Breakdown in Solids. Oxford: Clarendon Press; 1964.

[45] Kim WY, Lee YS, Lee HCh, Ka DY, Kim SY. Analysis of static imprint phenomenon in ferroelectric VDF-TrFE copolymer film for nonvolatile memory devices. Journal of the Korean Physical Society 2010;57(6) 1690-1694.

[46] Pertsev NA, Contreras JR, Kukhar VG, Hermanns B, Kohlstedt H, Waser R. Coercive field of ultrathin $Pb(Zr_{0.52}Ti_{0.48})O_3$ epitaxial films. Applied Physics Letters 2003;83(16) 3356-3358.

[47] Tagantsev AK, Stolichnov I, Setter N, Cross JS. Nature of nonlinear imprint in ferroelectric films and long-term prediction of polarization loss in ferroelectric memories. Journal of Applied Physics 2004;96(11) 6616-6623.

[48] Abe K, Yanase N, Yasumoto T, Kawakubo T. Voltage shift phenomena in a heteroepitaxial $BaTiO_3$ thin film capacitor. Journal of Applied Physics 2002;91(1) 323-330.

[49] Le Rhun G, Bouregba R, Poullain G. Polarization loop deformations of an oxygen deficient $Pb(Zr_{0.25}Ti_{0.75})O_3$ ferroelectric thin film. Journal of Applied Physics 2004;96(10) 5712-5721.

[50] He JQ, Vasco E, Jia CL, Wang RH. Direct observation of a fully strained dead layer at $Ba_{0.7}Sr_{0.3}TiO_3/SrRuO_3$ interface. Applied Physics Letters 2005, 87(6) 062901.

[51] Cillessen J, Prins M, Wolf R. Thickness dependence of the switching voltage in all-oxide ferroelectric thin-film capacitors prepared by pulsed laser deposition. Journal of Applied Physics 1997;81(6) 2777-2783.

[52] Tagantsev AK, Landivar M, Colla E, Setter N. Identification of passive layer in ferroelectric thin films from their switching parameters. Journal of Applied Physics 1995;78(4) 2623-2630.

[53] Hesse D, Alexe M. Ferroelectric nanostructures for future high-density non-volatile memory applications – preparation methods, microstructure, and physical properties, Autumn School, Berlin, 7. 10. 2005, http://crysta.physik.hu-berlin.de/as2005/pdf/as2005_talk_17_Hesse.pdf.

[54] Zubko P, Jung D J, Scott J F. Space charge effects in ferroelectric thin films. Journal of Applied Physics 2006;100(11) 114113.

[55] Fredrickson KD, Ponath P, Posadas AB, McCartney MR, Aoki T, Smith DJ, Demkov AA. Atomic and electronic structure of the ferroelectric $BaTiO_3$/Ge(001) interface. Applied Physics Letters 2014;104(24) 242908.

[56] Spaepen F. Interfaces and Stresses in Thin Films. Acta Materialia 2000;48 31-42.

[57] Wu WB, Wong KH, Choy CL. Interface-oxygen-loss-controlled voltage offsets in epitaxial $Pb(Zr_{0.52}Ti_{0.48})O_3$ thin-film capacitors with $La_{0.7}Sr_{0.3}MnO_3$ electrodes. Applied Physics Letters 2004;85(21) 5013-5015.

[58] Lian L, Sottos NR. Stress effects in sol-gel derived ferroelectric thin films. Journal of Applied Physics 2004;95(2) 629-634.

[59] Ma W, Cross LE. Strain-gradient-induced electrical polarization in lead zirconate titanate ceramics. Applied Physics Letters 2003;82(19) 3293-3295.

[60] Tuttle BA, Voigt JA, Garino TJ, Goodnow DC, Schwartz RW, Lamppa DL, Headley TJ, Eatough MO. Chemically prepared Pb(Zr, Ti)O_3 thin films: The effects of orientation and stress. In: Liu M, Safari A, Kingon A, Haertling G. (eds.) Proceedings Of the Eight International Symposium On Applications of Ferroelectrics, Greenwille USA, August 30 – September 2; 1992. p344-348.

[61] Alpay SP, Misirlioglu IB, Nagarajan V, Ramesh R. Can interface dislocations degrade ferroelectric properties? Applied Physics Letters 2004;85(11) 2044-2046.

[62] Koval V, Reece MJ, Bushby AJ. Enhanced ferroelectric loop asymmetry of lead zirconate titanate thin films under nanoindentation. Journal of Applied Physics 2007;101(2) 024113.

[63] Koval V, Reece MJ, Bushby AJ. Ferroelectric/ferroelastic behavior and piezoelectric response of lead zirconate titanate thin films under nanoindentation. Journal of Applied Physics 2005;97(7) 074301.

[64] Emelyanov AYu, Pertsev AN, Kholkin AL. Effect of external stress on ferroelectricity in epitaxial thin films. Physical Review B 2002;66(21) 214108.

[65] Kelman MB, McIntyre P, Hendrix BC, Bilodeau SM, Roeder JF. Effect of applied mechanical strain on the ferroelectric and dielectric properties of Pb($Zr_{0.35}Ti_{0.65}$)O_3 thin films. Journal of Applied Physics 2003;93(11) 9231-9236.

[66] Pertsev NA, Emelyanov A Yu. Domain-wall contribution to the piezoelectric response of epitaxial ferroelectric thin films. Applied Physics Letters 1997;71(25) 3646-3648.

[67] Gruverman A, Rodriguez BJ, Kingon AI, Nemanich RJ, Tagantsev AK, Cross JS, Tsukada M. Mechanical stress effect on imprint behavior of integrated ferroelectric capacitors. Applied Physics Letters 2003;83(4) 728-730.

[68] Lu H, Bark CW, Ojos D, Alcala J, Eom CB, Catalan G, Gruverman A. Mechanical writing of ferroelectric polarization. Science 2012;336 59-61.

[69] Salje EKH. Phase transitions in ferroelastic and co-elastic crystals. Cambridge University Press; 1993.

[70] Araki W, Malzbender J. Ferroelastic deformation of $La_{0.58}Sr_{0.4}Co_{0.2}Fe_{0.8}O_{3-\delta}$ under uniaxial compressive loading. Journal of the European Ceramic Society 2013;33(4) 805-812.

[71] Fett T, Munz D, Thun G. Nonsymmetric Deformation behavior of lead zirconate titanate determined in bending tests. Journal of the American Ceramic Society 1998;81(1) 269-272.

[72] Cao H, Evans AG. Nonlinear deformation of ferroelectric ceramics. Journal of the American Ceramic Society 1993;76(4) 890-896.

[73] Marsilius M, Webber KG, Aulbach E, Granzow T. Comparison of the temperature-dependent ferroelastic behavior of hard and soft lead zirconate titanate ceramics. Journal of the American Ceramic Society 2010;93(9) 2850-2856.

[74] Viola G, Verbylo D, Orlovskaya N, Reece MJ. Effect of composition on rate dependence of ferroelastic/ferroelectric switching in perovskite ceramics. Materials Science and Technology 2009;25(11) 1312-1315.

[75] Lugovy M, Slyunyayev V, Orlovskaya N, Verbylo D, Reece MJ. Room-temperature creep of $LaCoO_3$-based perovskites: Equilibrium strain under compression. Physical Review B 2008;78(2) 024107-9.

[76] Picht G, Webber KG., Zhang Y, Kungl H, Damjanovic D, Hoffmann MJ. Critical mechanical and electrical transition behavior of $BaTiO_3$: The observation of mechanical double loop behaviour. Journal of Applied Physics 2012;112(12) 124101.

[77] Plietsch R. Ehrlich K. Strength differential effect in pseudoelastic NiTi shape memory alloys. Acta Materialia 1997;45(6) 2417-2424.

[78] Xie Z, Liu Y, Humbeeck JV. Microstructure of NiTi shape memory alloy due to tension–compression cyclic deformation. Acta Materialia 1998;46(6) 1989-2000.

[79] Kassner ME, Geantil P, Levine LE, Larson BC. Backstress, the Bauschinger effect and cyclic deformation. Materials Science Forum 2009;604-605 39-51.

[80] Ren XB, Otsuka K. Universal symmetry property of point defects in crystals. Physical Review Letters 2000;85 1016-1019.

[81] Koval V, Skorvanek I, Yan H. Low-temperature magnetic and dielectric anomalies in rare-earth-substituted $BiFeO_3$ ceramics. Journal of the American Ceramic Society 2014;97(12) 3729-3732.

[82] Nogues J, Schuller Ivan K. Exchange bias. Journal of Magnetism and Magnetic Materials 1999;192(2) 203-232.

[83] Meiklejohn WH. Exchange anisotropy-A review. Journal of Applied Physics 1962;33(3) 1328-1335.

[84] Nogues J, Lederman D, Moran TJ, Schuller Ivan K. Positive Exchange bias in FeF_2-Fe bilayers. Physical Review Letters 1996;76(24) 4624-4627.

[85] Malozemoff AP. Random-field model of exchange anisotropy at rough ferromagnetic-antiferromagnetic interfaces. Physical Review B 1987;35(7) 3679-3682.

[86] Mauri D, Siegmann HC, Bagus PS, Kay E. Simple model for thin ferromagnetic films exchange coupled to an antiferromagnetic substrate. Journal of Applied Physics 1987;62(7) 3047-3049.

[87] Koon NC. Calculations of exchange bias in thin films with ferromagnetic/antiferromagnetic interfaces. Physical Review Letters. 1997;78(25) 4865-4868.

[88] Girgis E, Portugal RD, Loosvelt H, M. Van Bael J, Gordon I, Malfait M, Temst K, Van Haesendonck C. Enhanced asymmetric magnetization reversal in nanoscale Co/CoO arrays: Competition between exchange bias and magnetostatic coupling. Physical Review Letters 2003;91(18) 187202-4.

[89] Tian ZM, Yuan SL, Yin SY, Liu L, He JH, Duan HN, Li P, Wang CH. Exchange bias effect in a granular system of $NiFe_2O_4$ nanoparticles embedded in an antiferromagnetic NiO matrix. Applied Physics Letters 2008;93(22) 222505-3.

[90] Yuan SJ, Li L, Qi TF, DeLong LE, Cao G. Giant vertical magnetization shift induced by spin canting in a $Co/Ca_2Ru_{0.98}Fe_{0.02}FeO_4$ heterostructure. Physical Review B 2013;88(2) 024413-5.

[91] Nogues J, Leighton C, Schuller Ivan K. Correlation between antiferromagnetic interface coupling and positive exchange bias. Physical Review B 2000;61(2) 1315-1317.

[92] Watanabe H. Thermo-remanent magnetism in the systems La_2O_3-Fe2O3 and Nd_2O_3-Fe_2O_3. Journal of the Physical Society of Japan 1959;14(4) 511-516.

[93] Menyuk N, Dwight K, Wickham DG. Magnetization reversal and asymmetry in cobalt vanadate (IV). Physical Review Letters 1960;4(3) 119-120.

[94] Ohta K, Matsuyama T, Kajiura M, Teranishi T. Disaccommodation of magnetic permeability and induced anisotropy in amorphous Fe-Co alloys. Journal of Magnetism and Magnetic Materials 1980;19(1-3) 165-167.

[95] Kohmoto O, Yamaguchi N, Ohya K, Fujishima H. Change of the magnetic property in some amorphous alloys by low temperature annealing. Japanese Journal of Applied Physics 1978;17(1) 257-258.

[96] Rivas M, García JA, Tejedor M, Bertrán E, Céspedes JG. Influence of the dipolar interactions in the magnetization reversal asymmetry of hard–soft magnetic ribbons. Journal of Applied Physics 2005;97(2) 023903-5.

[97] Skomski R, Zhou J, Kirby R, Sellmyer DJ. Magnetic aging. In: Chipara M, Puglisi O, Skomski R, Jones F, Hsiao B. (eds.) Proceedings of the Materials Research Society 2006, Symposium 887; 133-138.

[98] Moskowitz BM. Magnetic viscosity, diffusion after-effect, and disaccommodation in natural and synthetic samples. Geophysical Journal International 1985;82(2) 143-161.

IntechOpen